DESIGN OF MULTIPLE-OUTPUT FLYBACK CONVERTER WITH INDEPENDENTLY CONTROLLED OUTPUTS FOR TV POWER SUPPLY

A Thesis

by

Ramazan Düzgün

Submitted to the
Graduate School of Sciences and Engineering
In Partial Fulfillment of the Requirements for
the Degree of

Master of Science

in the
Department of Electrical and Electronics Engineering

Özyeğin University
May 2023

DESIGN OF MULTIPLE-OUTPUT FLYBACK CONVERTER WITH INDEPENDENTLY CONTROLLED OUTPUTS FOR TV POWER SUPPLY

Advisor: Asst. Prof. Mehmet Parlak, Özyeğin University
Coadvisor: Dr. İsmail Yılmazlar, Özyeğin University

Approved by:

Asst. Prof. Mehmet Parlak, Advisor
Department of Electrical and Electronics Engineering
Özyeğin University

Prof. Dr. Duygun Erol Barkana
Department of Electrical and Electronics Engineering
Yeditepe University

Asst. Prof. Ahmet Tekin
Department of Electrical and Electronics Engineering
Boğaziçi University

Date Approved: 18 May 2023

To benefit of the world.

ABSTRACT

This study presents the design of a multiple-output flyback converter (MOFC) with independently controlled outputs for a television power supply system. The proposed converter is capable of independently controlling the output voltage and output current of multiple outputs, allowing for efficient and precise power delivery to various subsystems within the TV. The current of the backlight LEDs and the system supply voltage are controlled independently, and the backlight LEDs are directly fed from the same flyback transformer, eliminating the need for a buck or boost converter stage. The 12V system voltage is regulated by an additional N-MOSFET. Thanks to the absence of an extra converter stage and the use of small transformer sizes, both card sizes and costs are reduced while achieving higher peak efficiency and power density. The simulation and experimental designs of the proposed model are explained in detail, and the results are shared. Regulation of both outputs is achieved and measured. The worst regulation of the outputs is measured when the 12V output voltage ripple level is %5.61 when both output loads are light. At full loading conditions, the ripple level of 12V is measured %2.28. Thermal measurements are done in room conditions at full loading conditions at an input voltage of 230VAC. The peak temperature is noted 74.0 Celcius on the flyback MOSFET. Power card sizes are reduced by %28.8 and the BOM cost is decreased by 0.46 USD and the peak efficiency is measured %90.85 which is increased by %1.35 in comparison to the conventional card.

ÖZETÇE

Bu çalışma, bir televizyon güç kaynağı sistemi için çıkışları bağımsız control edilen çok çıkışlı bir flyback dönüştürücü tasarımını sunmaktadır. Önerilen dönüştürücü, TV içindeki çeşitli alt sistemlere verimli ve hassas güç dağıtımına izin vererek, çoklu çıkışların çıkış voltajını ve akımını bağımsız olarak kontrol etme yeteneğine sahiptir. Arka ışık LED'lerinin akımı ve sistem besleme gerilimi bağımsız olarak kontrol edildi ve arka ışık LED'leri doğrudan aynı flyback trafosundan beslenerek bir düşürücü veya yükseltici dönüştürücü aşamasına olan ihtiyacı ortadan kaldırıldı. 12V sistem voltajı ek bir N-MOSFET tarafından regüle edildi. Ekstra bir dönüştürücü aşamasının olmaması ve küçük transformatör boyutlarının kullanılması sayesinde, daha yüksek tepe verimliliği ve güç yoğunluğu elde edilirken, hem kart boyutları hem de maliyetler azaltıldı. Önerilen modelin simülasyonu ve deneysel tasarımı detaylı bir şekilde anlatılmış ve sonuçlar paylaşılmıştır. Her iki çıktının regülasyonu sağlandı ve ölçüldü. Çıkışların en kötü regülasyonu, her iki çıkış yükü de hafifken 12V çıkış voltajı dalgalanma seviyesi %5.61 olduğunda ölçüldü. Tam yük koşullarında, 12V dalgalanma seviyesi %2.28 olarak ölçüldü. Termal ölçümler oda koşullarında 230VAC giriş voltajında tam yük koşullarında yapıldı. En yüksek sıcaklık, flyback MOSFET'inde 74.0 Celcius olarak not edildi. Geleneksel karta kıyasla güç kartı boyutları %28,8 oranında küçüldü, BOM maliyeti 0,46 USD azaldı ve en yüksek verimlilik %1,35 artarak %90,85 olarak ölçüldü.

ACKNOWLEDGEMENTS

Firstly, I would like to thank my advisors Mehmet Parlak and İsmail Yılmazlar for their precious help. I also would like to thank my colleagues at Vestel Electronics, family, and best friends for their support during the writing process of this thesis.

Table of Contents

List of Tables

List of Figures

Chapter I

INTRODUCTION

1.1 History of TVs

The engineer and inventor John Logie Baird invented the first television (TV) in the 1920s [1]. Since then, TVs have been developed worldwide. In the 1950s, with the introduction of color TVs, they became a staple furniture item in households [2]. The classification of displays is represented in Figure 1.

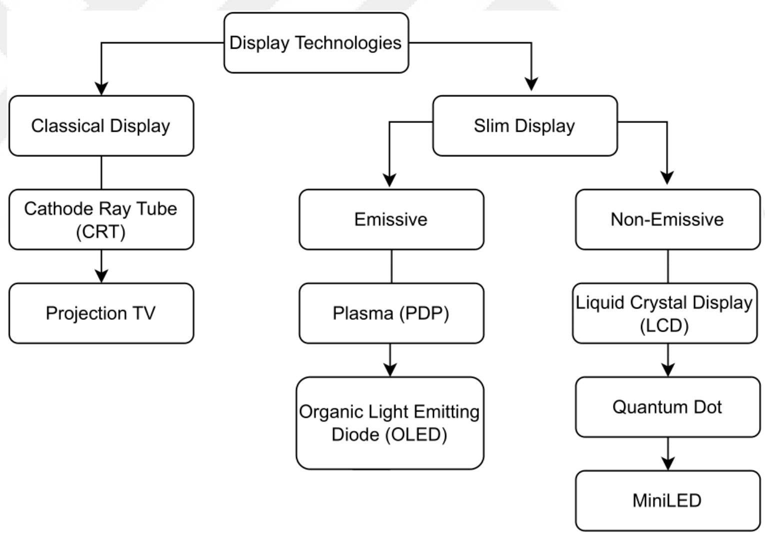

Figure 1 Classification of display technologies

Classical displays primarily include CRT and projection TVs. CRT TVs utilize electron guns at the rear to generate light. To accelerate the electrons toward the TV screen, a flyback transformer generates a high voltage at the anode. The electrons pass through the heated cathode tube and collide with the phosphor surface on the screen, resulting in the illumination of the TV screen [3]. The basic structure of a CRT is illustrated in Figure 2. CRT TVs offer advantages such as fast response times and vibrant colors. However, they tend to be heavier, have lower resolution, and consume more power compared to LCD TVs.

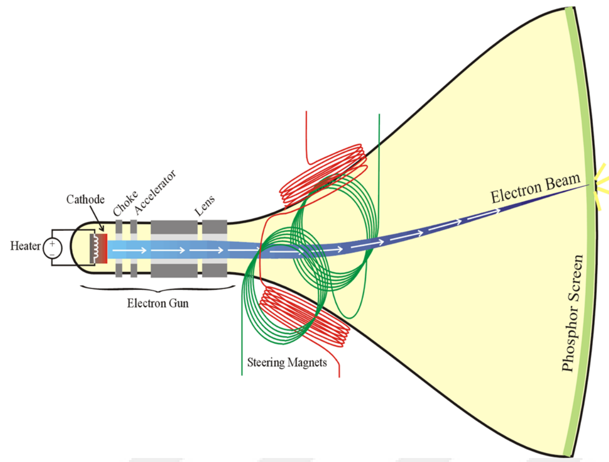

Figure 2 Basic structure of CRT TV[23]

Projection TVs utilize the digital light processing (DLP) system, which employs over a million micromirrors to direct light through the screen [4]. However, projection TVs typically have lower contrast ratios and resolutions compared to LCD displays. The structure of a projection TV is depicted in Figure 3.

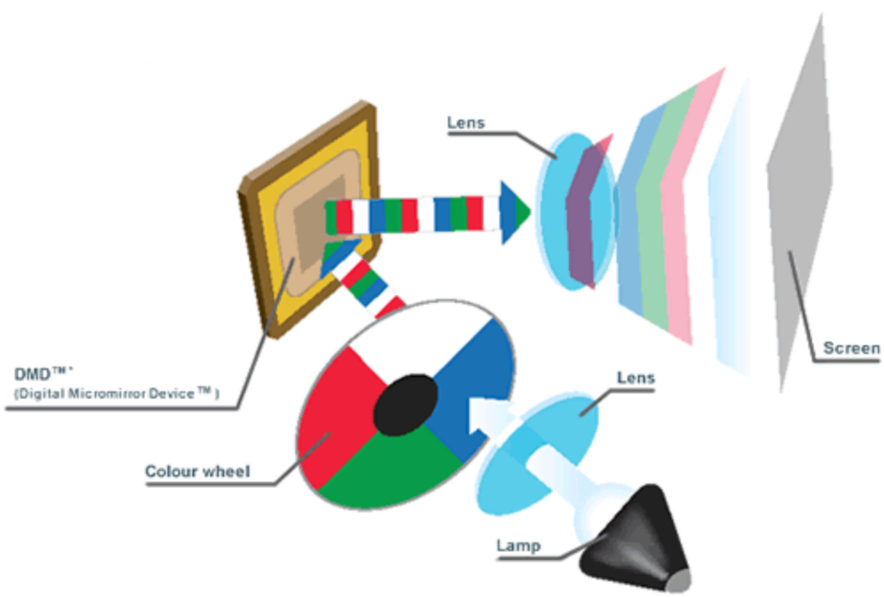

Figure 3 Basic structure of projection TV[24]

In the slim display technology category, plasma TVs were among the most impressive large-screen TVs available in the market due to their wide viewing angles, fast response times, high dynamic contrast ratios, and thin form factor. Each pixel in a plasma TV typically contains three electrodes: the scan (Y), sustain (X), and address (A) electrodes, as depicted in Figure 4. These pixels work together to create a full-color image, with individual subpixels for red, green, and blue [5][6]. However, one disadvantage of plasma TVs is their relatively high power consumption.

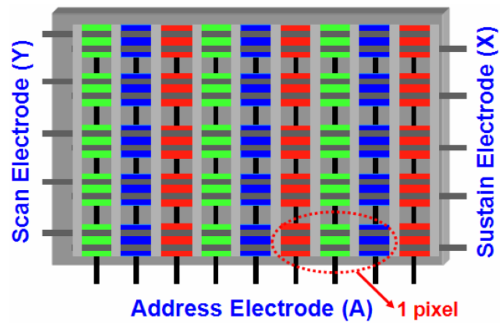

Figure 4 Basic structure of plasma TV[6]

The OLED display represents the most advanced display technology available today, offering exceptional picture quality and installation flexibility. Unlike LCD displays, OLED panels do not require a separate backlighting system. Instead, each individual pixel emits its own light, resulting in vibrant and accurate colors. Furthermore, the self-luminous nature of OLED displays allows for deeper blacks, leading to an outstanding contrast ratio. Figure 5 provides a comparison between the structures of OLED and LCD displays, highlighting the differences between the two technologies.

LCD displays have been an integral part of our daily lives for over 40 years. They find extensive use in various devices such as mobile phones, notebook PCs, video equipment, TVs, and navigation systems [8]. In LCD TVs, LEDs serve as the backlight units, as depicted in Figure 5, due to their efficiency, reliability, and ability to facilitate thinner TV designs. The pixels of an LCD TV contains liquid crystals that require energization to form an image on the screen. As the pixels do not have a light source, the backlight LEDs illuminate them, allowing us to see the image displayed on the screen. LED TVs offer compactness, low power consumption, thin

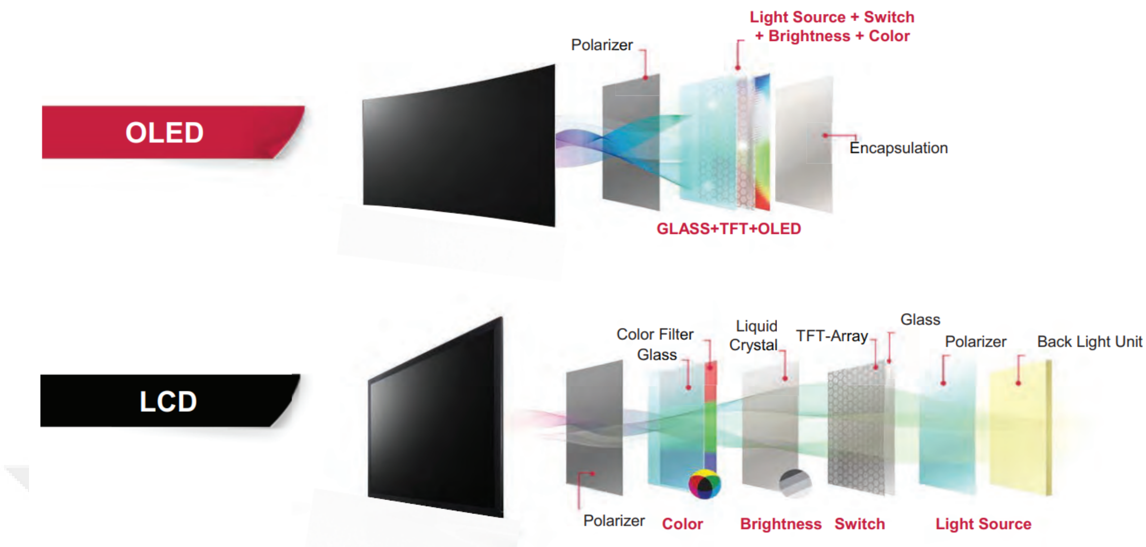

Figure 5 OLED and LCD display structures[7]

profiles, and operation at low voltages. However, they do have drawbacks, including lower contrast ratios and slower response times [9].

Currently, LED TVs continue to dominate the television market. LED panels are extensively used in indoor and outdoor applications, ranging from 22" to 108" TVs, as well as visual solution (VS) platforms. These LED panels are supplied power by an isolated power supply card. The luminance level of the LEDs is determined by the current drawn by them. Therefore, the power supply card is responsible for controlling the supplied current to the LEDs. This thesis aims to investigate the design of a power supply card specifically for LED TVs up to 43" in size. A novel design will be proposed, accompanied by a detailed explanation of its working principles, operational stages, and design considerations. The thesis will present simulation results as well as hardware implementations and their corresponding outcomes.

1.2 Motivation

The power supply card of a TV typically provides power to both the mainboard and the backlight unit. The mainboard of the TV generally requires a voltage level ranging from 12V to 13.2V, which is typically supplied directly by the main converter transformer. On the other hand, the voltage levels required by the backlight unit can vary based on the panel size and screen technology. The conventional power supply cards for LED TVs utilize cascaded DC-DC converter structures, such as boost converters and buck converters, to supply the backlight unit. This structure generates the necessary voltage level for the backlight and regulates the current flowing through the LEDs to achieve the desired luminance. However, this cascaded structure has drawbacks, including reduced efficiency, increased space requirements on the power card, and higher costs.

The primary motivation is to enhance efficiency while reducing the size of the power card and the overall bill of materials (BOM) costs. This can be achieved by proposing a new method to supply the TV backlight directly from the main converter transformer, eliminating the need for an additional cascaded DC-DC converter block.

Chapter II

LITERATURE RESEARCH

2.1 DC-DC Converters with Isolation

TV power supplies are required to adhere to safety and reliability standards, which include the provision of electrical isolation. This isolation is crucial for protecting end-users from electric shock hazards. As depicted in Figure 6, electrical isolation in TV power supplies is typically achieved through the use of a high-frequency (HF) transformer [10]. The HF transformer ensures that there is no direct electrical connection between the input and output sides of the power supply, maintaining the necessary safety measures.

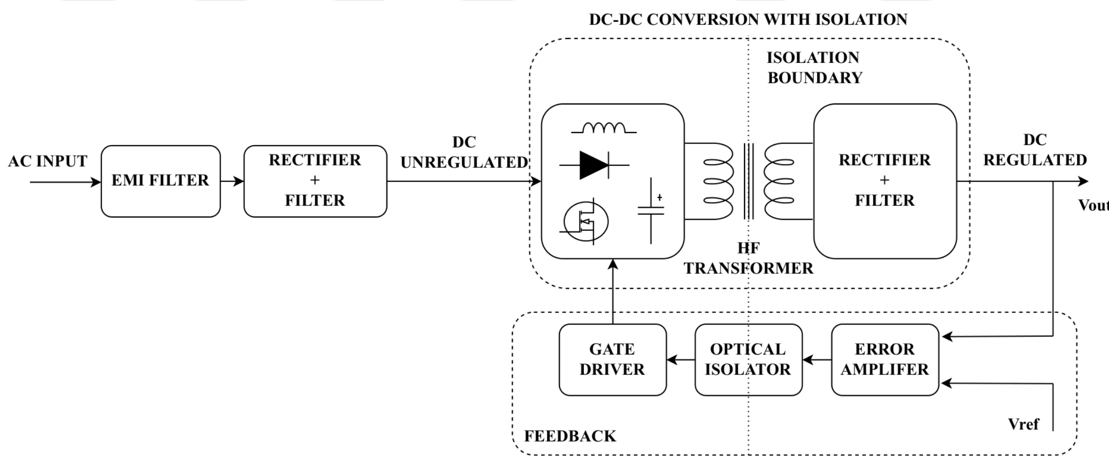

Figure 6 Isolated DC-DC power supply schematic

A conventional isolated DC-DC power supply typically comprises a rectifier, a filter, a switching device, a transformer, and a feedback circuit. The specific component count, ratings, switching frequency, magnetic elements, and filters can vary depending on the chosen topology.

When designing a TV power supply, it is crucial to select the appropriate topology.

This selection process should begin with determining the power requirements of the system. Table 1 presents various topologies based on power levels and certain ratings, offering options for consideration. In this thesis, flyback topology is selected.

Table 1 Topology selection guide[11]

Parameters	Flyback	Forward	Half Bridge	Full Bridge
Switch Voltage Rating	$2V_{IN}$	$2V_{IN}$	V_{IN}	V_{IN}
Switch Peak Current	$4V_{IN}$	$2P_{IN}/V_{IN}$	$2P_{IN}/V_{IN}$	P_{IN}/V_{IN}
Diode Voltage Rating	$2V_{OUT}$	$2V_{OUT}$	$2V_{OUT}$	$2V_{OUT}$
Transformer Relative Core Size	1.62	1.4	1.00	1.00
Power Limit (W)	100	200	500	2000

2.1.1 Transformer Models

HF transformers used in DC power supplies serve two primary functions: providing electrical isolation between the primary and secondary sides and stepping up or stepping down applied voltages and currents [12].

The cores of HF transformers are typically made from ferromagnetic materials. The typical characteristics of a transformer core can be represented by the B-H loop, as shown in Figure 7. In this loop, B_{sat} represents the maximum flux density limit that the core can withstand before it saturates, and B_r represents the residual magnetic flux density that remains after demagnetization.

The magnetic flux density, represented by B, can be defined as the product of magnetic permeability and the magnetic field intensity H. Mathematically, this relationship can be written as:

$$B = \mu_0 \times \mu_r \times H \tag{1}$$

where H represents the magnetic field intensity, B is the magnetic flux density, μ_0 is the magnetic permeability of free space and μ_r is the magnetic permeability of the medium.

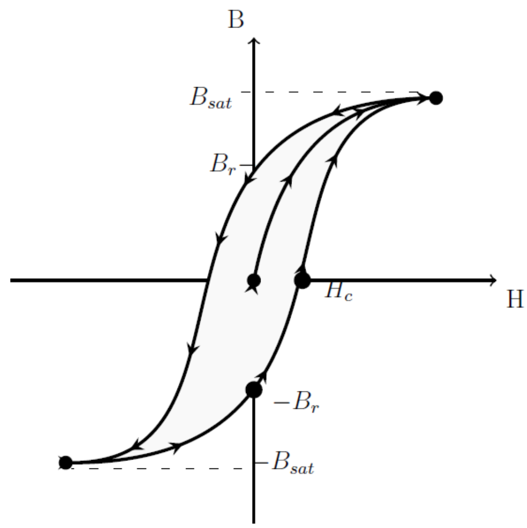

Figure 7 B-H hysteresis of a transformer core[13]

When the excitation of the HF transformer is sinusoidal, the resulting magnetic flux in the core also becomes sinusoidal. As the magnetic field intensity (H) increases, as indicated by the arrows on the curve in Figure 7, the magnetic flux density (B) rises until it reaches the saturation point (B_{sat}). Then, as the magnetic field intensity decreases, B follows a different path and approaches the residual magnetic flux density (B_r). Even when H reaches zero, the maximum flux density remains at B_r. This residual magnetic flux persists within the core material. Only a specific negative value of H can fully eliminate this residual B. This characteristic behavior of magnetic core materials is known as the hysteresis B-H loop [13].

The basic structure of a two-winding transformer and its equivalent circuit model are depicted in Figure 8. In many power electronics circuits, the equivalent model can be utilized by neglecting factors such as leakage inductance, core resistance, and copper resistance. The equivalent model allows for the representation of the transformer in the circuit. In this model, L_M represents the magnetizing inductance. The input-output relationships can be expressed as follows:

$$\frac{v_1}{v_2} = \frac{N_1}{N_2} = n \tag{2}$$

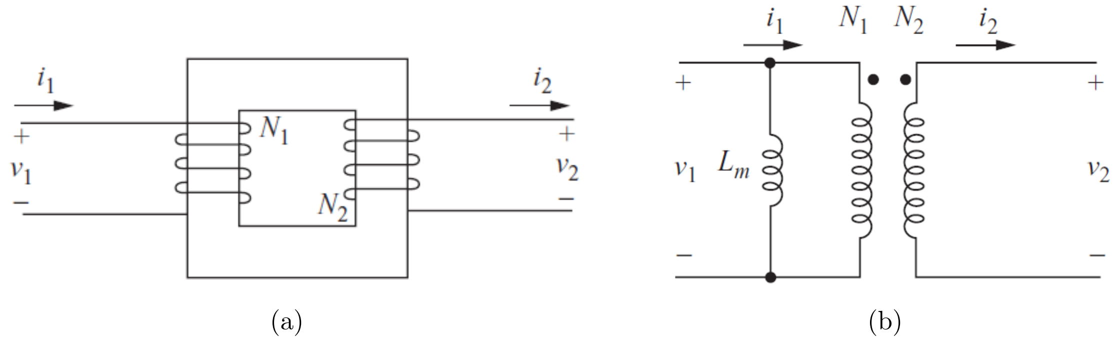

Figure 8 Transformer representation: (a)two-winding transformer; (b) equivalent circuit model [12]

$$\frac{i_1}{i_2} = \frac{N_2}{N_1} = \frac{1}{n} \tag{3}$$

where N_1 is the number of turns of the primary winding and N_2 is the number of turns of the secondary winding, and n is the turns ratio.

According to equations (2) and (3), the voltage ratio is the inverse of the current ratio. This relationship arises due to the dot convention, as illustrated in Figure 8(b). The dots indicate the winding directions and represent the polarity between the two windings. In the primary side, the dotted terminal is considered positive, and correspondingly, on the secondary side, the dotted terminal voltage is also positive. When the current enters the primary side through the dotted terminal, it can be said that the current leaves the dotted terminal on the secondary side in accordance with the turns ratio. This dot convention ensures that the voltage and current relationships are consistent with the winding polarities and turns ratio of the transformer.

2.1.2 Flyback Converter

The flyback converter has been a popular choice for industrial applications for many years. It is a commonly used topology for low-power DC-DC switch mode power supplies (SMPS). The flyback converter offers several advantages, including simplicity in design, low cost, good electromagnetic interference (EMI) performance, support for multiple outputs, and high efficiency. It is particularly favored as a topology for TV power supplies with power ratings below 80W.

The operation of the flyback converter is based on a coupled inductor that transfers power from the primary side to the secondary side while providing electrical isolation between the input and output. This characteristic makes it suitable for offline converter applications[22]. A conventional Flyback converter is depicted below

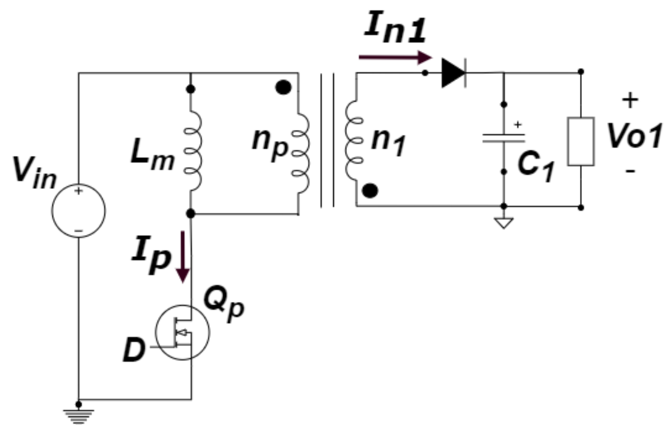

Figure 9 Conventional flyback converter circuit

in Figure 9. Basically, it contains a dc-link capacitor, transformer, switching mosfet, rectifier diode, and output capacitor. Energy is stored in the magnetizing inductance of the transformer during the primary switch is ON state. Primary current linearly rises up since input voltage is constant. When the switch turns off, the stored energy is transferred to the secondary winding. At this sudden, the diode is forward-biased because of the polarity of winding, and the current flow is allowed to charge the output capacitors. During the primary is ON state, the load is fed from charged output capacitors[10][12].

In the flyback converter, the input-output voltage relationship is given in eq. 4.

$$V_{o1} = V_{in} \times \frac{n_1}{n_P} \times \frac{D}{1 - D} \tag{4}$$

where n_p and n_1 are primary and secondary number of turns respectively. D is the duty cycle which is the ratio of the primary switch on time to the switching period.

2.1.3 Forward Converter

Forward converter topology is also one of the most used topologies usually for low and medium power applications. This converter is actually derived from a buck converter topology[14]. The winding structure of a forward converter transformer is quite different from a flyback converter transformer. As shown in Fig. 10, there are three windings: n_p and n_s are transferring energy from primary to secondary when the primary switch is turned on; n_r is the reset winding that reduce the magnetizing current to zero when the primary switch is turned off[12].

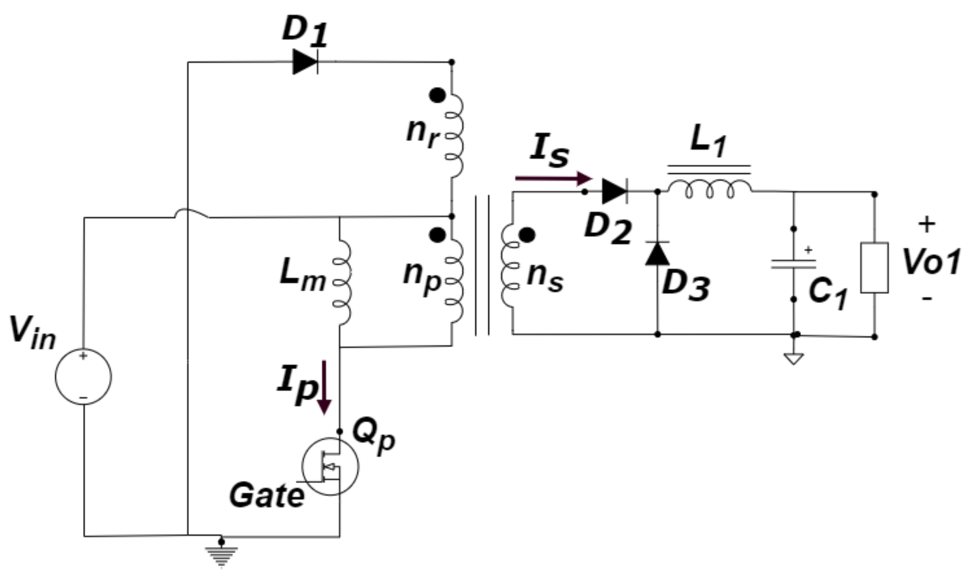

Figure 10 Conventional forward converter circuit

Unlike the flyback converter, the dotted terminals are not inverse. When the primary switch is turned on, the dotted terminal on the primary side is positive, so the dotted terminal on the secondary is also positive which makes the D_2 forward-biased. The primary current I_P increases linearly, and energy is transferred to the secondary onto L_1 and C_1 filter block and to the load through the diode D_2.

When the primary switch is turned off, the polarity of the n_p and n_s voltages reverses. Thus D_2 is reverse-biased, but D_1 and D_3 are forward-biased. D_3 is the free-wheeling diode. Since D_3 is forward-biased, the energy is transferred to the load through the inductor L_1. During the diode D_1 conducts, the magnetizing inductance current flows back to the input and resets the core energy[15].

In the forward converter, the input-output voltage relationship is given in eq. 5.

$$V_o = V_{in} \times D \times \frac{n_S}{n_P} \tag{5}$$

The forward converter transfers the energy from primary to secondary when the primary switch is closed. Unlike the flyback converter, the forward converter does not store the energy in L_M. So the magnetizing inductance of the forward converter is not included in the input and output relationship[12]. Since the forward converter does not store energy in the transformer, the transformer size may be smaller than that of the same power-level flyback converter transformer[15].

2.1.4 The Push-Pull Converter

Fig. 11 shows the conventional push-pull converter circuit. A square-wave ac voltage is produced at the input by the operation of the primary switches Q_1 and Q_2. On the secondary side, a center-tapped structure is used, thus there is only one diode voltage drop during the operation.

When Q_1 is turned on, diode D_2 is forward-biased, D_1 is reverse-biased, and current I_{L1} is linearly increase and charge the capacitor. When Q_2 is turned on, diode D_1 is forward-biased, D_2 is reverse-biased, and current I_{L1} is linearly increase and charge the capacitor. When both primary switches are turned off, there is no current flow on the primary windings. Voltage polarity of the inductor L_1 is reversed and D_1 and D_2 are forward-biased. The current of the inductor L_1 linearly decreases since the voltage across the L_1 is equal to the negative of the constant output voltage.

In the push-pull converter, the input-output voltage relationship is given in eq. 6.

$$V_o = 2 \times V_{in} \times \frac{n_S}{n_P} \times D \tag{6}$$

where D is the duty cycle of each primary switch.

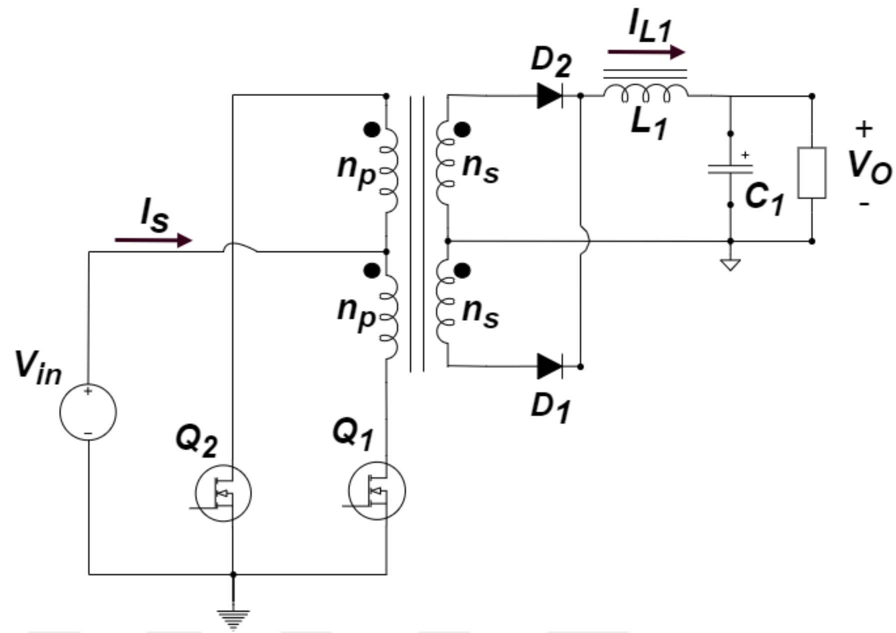

Figure 11 Conventional push-pull converter circuit

2.1.5 Half Bridge Converter

The half-bridge converter is another isolated dc-dc converter that is widely used in the industry. On the primary side, series coupling capacitors are located that minimize the dc component of the return current to the primary as can be seen in Fig. 12, thus the core saturation problems are minimized. Since the primary switches are driven alternatively, the voltage of the primary winding is always half of the input voltage. The voltage stresses of the primary switches are equal to the input voltage. Low voltage rating transistors can be used in primary. The disadvantage of this converter is, the source of the primary switch Q_1 is not at the ground level of the circuit, but is at high-ac level. The gate driver of this transistor must be isolated from the ground[14][15].

When Q_1 is on and Q_2 is off, the rectifier diode D_2 is forward-biased and diode D_1 is reverse-biased. The primary winding voltage is half of the input voltage, so the primary current increases linearly and stores energy in the primary winding. Since the D_2 is forward-biased, energy is directly transferred to load over the inductor L_1.

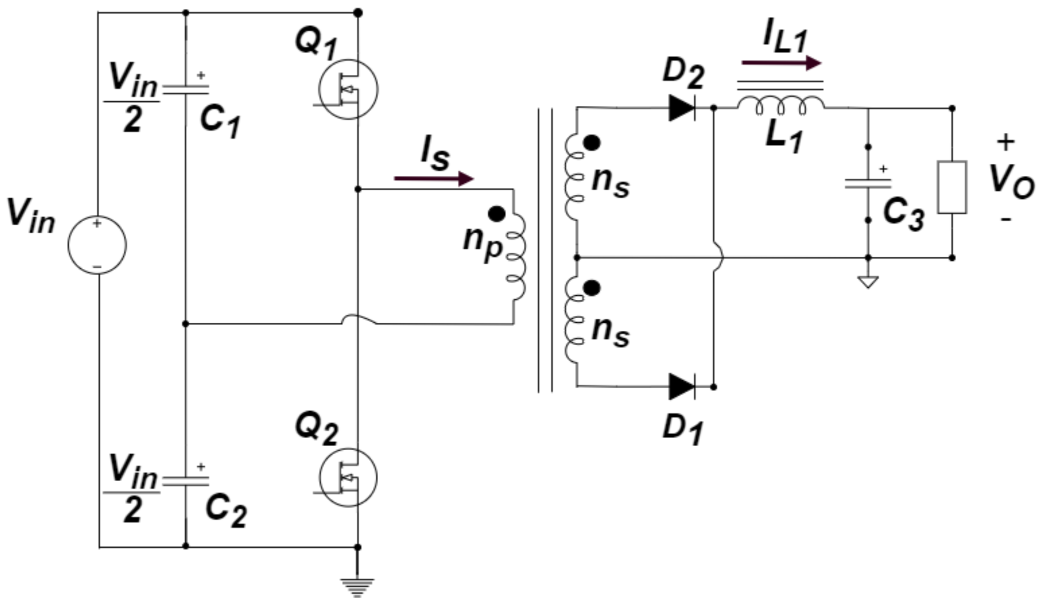

Figure 12 Conventional half-bridge converter circuit

When both primary switches Q_1 and Q_2 are off, same as the push-pull converter, there is no current flow on the primary windings. Voltage polarity of the inductor L_1 is reversed and D_1 and D_2 are forced to be forward-biased. The current of the inductor L_1 linearly decreases since the voltage across the L_1 is equal to the negative of the constant output voltage.

When Q_2 is on and Q_1 is off, the polarity of the primary winding voltage is reversed, therefore the rectifier diode D_1 is forward-biased and diode D_2 is reverse-biased. The primary current starts to build up and transfer the energy directly to the secondary winding[15].

In the half-bridge converter, the input-output voltage relationship is given in eq. 7.

$$V_o = V_{in} \times \frac{n_S}{n_P} \times D \tag{7}$$

where D is the duty cycle of each primary switch.

2.2 *Modes of Operation*

HF transformer that is used in flyback circuits stores the energy in the transformer during the primary switch is on as shown in Fig. 13(a), and transfers it to the secondary when the switch is turned off as shown in Fig. 13(b). In Fig. 13 faded lines represent there is no current flow, open circuit, solid lines represent there is a current flow. The behavior of the inductor current determines the mode of operation. If the inductor current does not decrease to zero and stays always positive, this mode is continuous conduction mode (CCM). However, the inductor current decrease to zero and beyond, this mode is discontinuous conduction mode (DCM). There is a boundary between CCM and DCM where the inductor current decreases to zero and raise up again at the start of the next cycle. This mode is called transition mode or boundary mode.

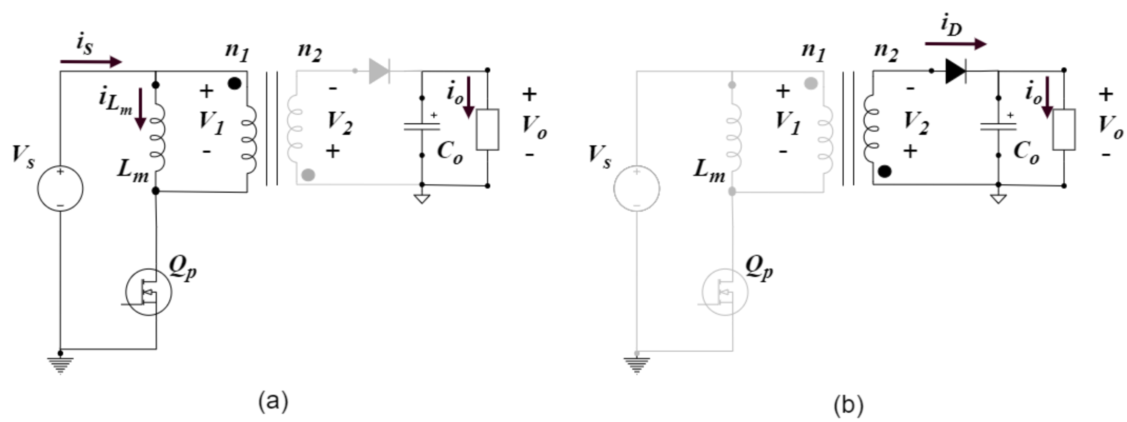

Figure 13 Operation of a flyback converter: (a) primary switch is ON; (b) primary switch is OFF

All operation modes are analyzed according to steady-state operation, input power and output power are equal. Also, leakage inductance, stray capacitors, core losses, and copper losses are neglected.

2.2.1 Continuous Conduction Mode

In CCM, energy is stored in the transformer by the primary current ramps up during on-time (DT), then the energy is not fully dissipated during off-time ($T - DT$). There is still current in the transformer and never falls to zero. The inductor current remains positive and flows continuously. The voltage and current waveforms of CCM operation are shown in Fig. 14.

Average source current I_S is related to the average of inductor current I_{LM}. It can be calculated from the triangle in the waveform of i_s as shown in Fig. 14. It's expressed in eq. 8.

$$I_S = \frac{I_{LM} \times DT}{T} = I_{LM} \times D \tag{8}$$

The change in inductor current can be written as,

$$\Delta i_{LM} = \frac{V_S \times DT}{L_M} \tag{9}$$

The peak of the inductor current is expressed as follows;

$$I_{LM,max} = I_{LM} + \frac{\Delta i_{LM}}{2} \tag{10}$$

CCM mode of operation advantages are small ripple and RMS current, lower switching loss, lower core loss, and smaller EMI filter and output filter. On the other hand, difficulty control, low light-load performance, and higher voltage stress on the secondary diodes are the disadvantages of it[16].

2.2.2 Discontinuous Conduction Mode

In DCM, the energy is stored in the transformer during on-time same as in CCM, but it is dissipated by the load completely during off-time. The inductor current falls to zero and stays zero before the start of the next cycle as shown in Fig. 15.

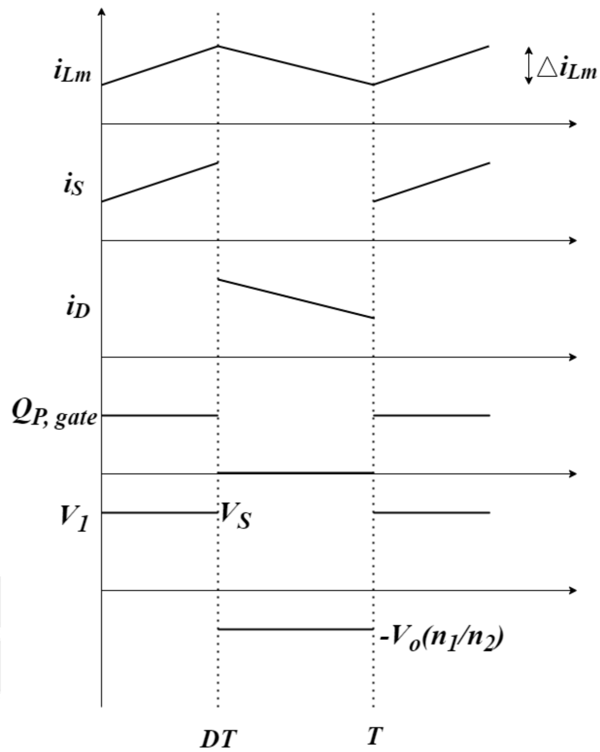

Figure 14 CCM operation of a flyback converter

Since the inductor current start at zero, the required output power must be produced until the current reaches the peak value. This causes a higher RMS and peak current than CCM. The peak inductor current is obtained from the area of the triangle in the waveform of i_{LM} shown in Fig. 14.

$$I_{LM,max} = \Delta i_{LM} = \frac{V_S \times DT}{L_M} \tag{11}$$

The average source current can be calculated from the area of the triangle in the waveform of i_{LM} shown in Fig. 15.

$$I_S = \frac{V_S \times DT}{L_M} \times DT \times \frac{1}{2} \times \frac{1}{T} = \frac{V_S \times D^2 T}{2L_M} \tag{12}$$

The advantages of DCM are ease of control, lower inductance allows small transformer design and no diode reverse recovery losses. The disadvantages of DCM are large ripple and peak current, higher switching losses, higher core loss, and large EMI filter and output filter[16].

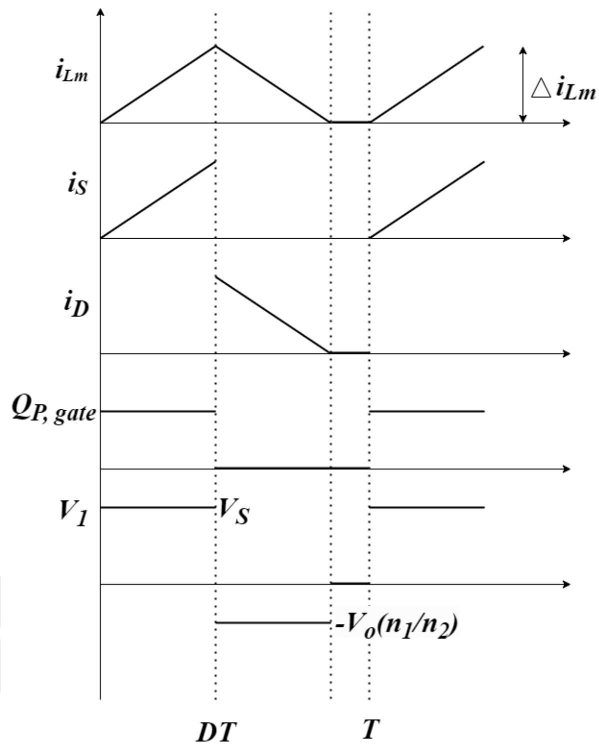

Figure 15 DCM operation of a flyback converter

2.2.3 Boundary of CCM and DCM

In boundary mode, the inductor current falls to zero at the end of the switching period and the next switching cycle begins at this instant. In boundary mode, the voltage and the current waveforms are shown in Fig. 16.

From the waveform in Fig. 16, the average inductor current,

$$I_{LM} = \frac{1}{2}\Delta i_{LM} = \frac{V_S \times DT}{2L_M} \tag{13}$$

The advantages of boundary mode are no diode reverse-recovery losses, lower inductance that allows the designing of a small transformer, and ease of control. Besides these, the disadvantages of boundary mode are large ripple and peak current, high core loss, high switching loss, large EMI filter, and output filter[16].

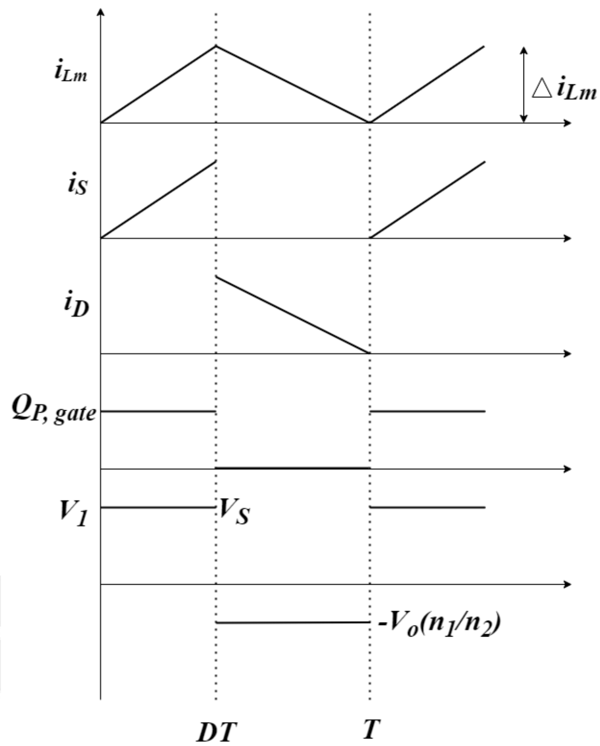

Figure 16 Boundary mode operation of a flyback converter

2.3 Multiple Output Flyback Converter

The power supply system of a television (TV) is responsible for delivering reliable and precise power to various subsystems within the TV, such as the display, audio, and control circuits. Conventional power supply designs often utilize multiple transformers and voltage regulators to provide isolation and voltage regulation for each subsystem, resulting in a complex and costly system.

To address these issues, multiple-output flyback converters have been proposed as a potential solution for TV power supply systems. These converters utilize a single flyback transformer and multiple control loops to provide electrical isolation and power conversion for multiple output rails. The ability to independently control the output voltage of each rail allows for efficient and precise power delivery to the various subsystems within the TV.

The MOFC (Multiple Output Flyback Converter) is one of the most used SMPS structures for low-power and isolated applications. The MOFC has wide usage areas such as TVs, computer power supplies, electric vehicles, military applications, and telecommunication systems [17]. However, in general, the main output is regulated and the other output is not regulated tightly. The non-regulated output tracks the regulated output, so it is acceptable only for light loads or it must be used with a post regulator or an additional converter structure.

2.3.1 Conventional MOFC Model

The block diagram of the conventional model is shown in Fig. 17. This conventional model consists of a flyback and a boost converter stage. The LED winding output of the flyback converter which is the input of the boost converter is non-regulated. To get a regulated and controlled LED current, there is used boost converter and controlled by LED driver IC. The flyback is controlled by the feedback of the main 12V system output voltage.

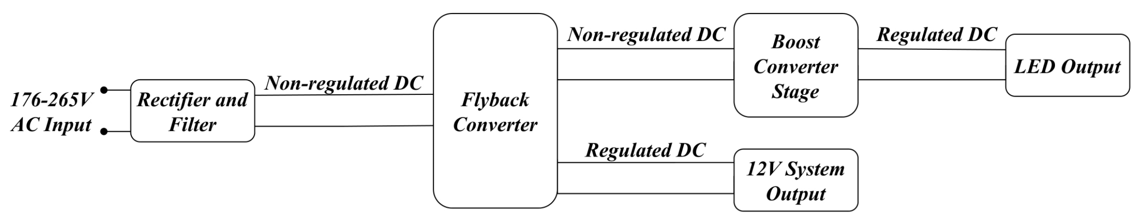

Figure 17 Conventional MOFC Block Diagram for TV Power Supply

The luminance level of the screen depends on the amount of current that flows through the LEDs of the TV backlight unit. LEDs' current is controlled by the LED driver controller IC. In conventional MOFC, the LED driver stage is a boost converter to get demanded regulated current and voltage for the LEDs. As shown in Fig. 18, the boost converter contains an inductor, a MOSFET, a diode, and an output capacitor.

The working principle of conventional MOFC is the same as conventional Single-Output Flyback Converter. The main output is regulated by monitoring the output

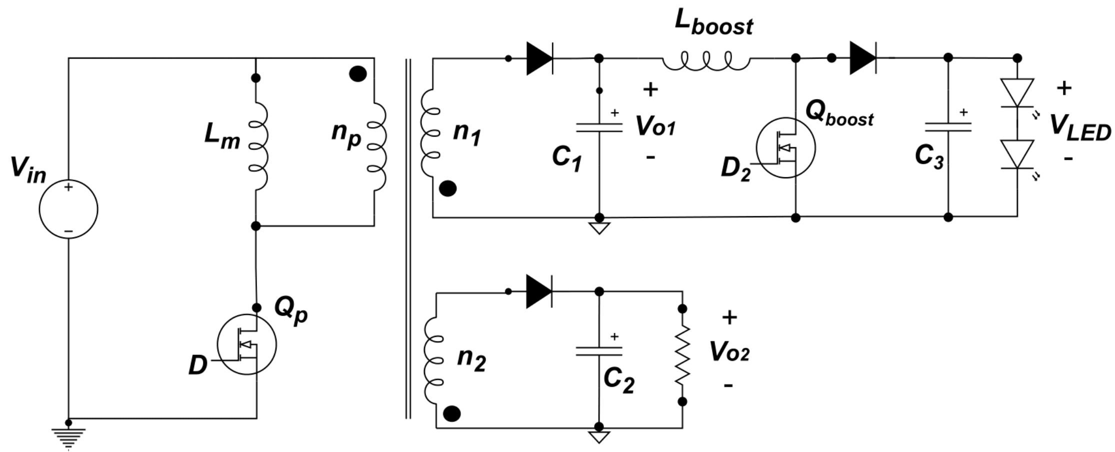

Figure 18 Conventional MOFC schematics for TV Power Supply

voltage, and the controller generates a PWM signal for the primary switch. Other outputs are not regulated and they only track the main output regulation, so they are affected by load changes on the main output. Energy is stored in the magnetizing inductance of the transformer during the primary switch is ON. Primary current linearly rises up since the input voltage is constant. When the switch turns off, the stored energy is transferred to the secondary and tertiary windings. At this instant, secondary diodes are forward-biased because of the polarity of windings, and the current flow is allowed to charge the output capacitors.

Due to one of the outputs being non-regulated, the conventional MOFC is used with an extra converter stage. This additional converter stage regulates and controls the LEDs' current of the TV Backlight. However, it decreases the efficiency while increasing the card sizes, the number of component count, and costs.

Several methods are presented to regulate the MOFC outputs fully. In [18] independent control of two outputs with two transistors is presented. One controller, one diode, and one switching device are needed for each regulated output, which means a high component count and cost. In [17] GaN HEMTs are used as SRs instead of diodes. The number of components is low and converter efficiency is %86.9. However, since they have no current regulated output, both presented methods are incompatible with supplying controlled current to the LEDs of the TV backlight unit.

This thesis proposes a new design of MOFC for TV power supply with independently controlled two outputs for better efficiency and higher power density. The proposed model is designed to supply a LED TV, therefore one of the outputs that supply the TV backlight LEDs is current controlled, and the other output that supplies the 12V TV system voltage is voltage controlled.

2.3.2 Proposed MOFC Model

Fig. 19 shows the block diagram of this new model that proposes a one-stage flyback topology to supply a LED TV with independently regulated outputs.

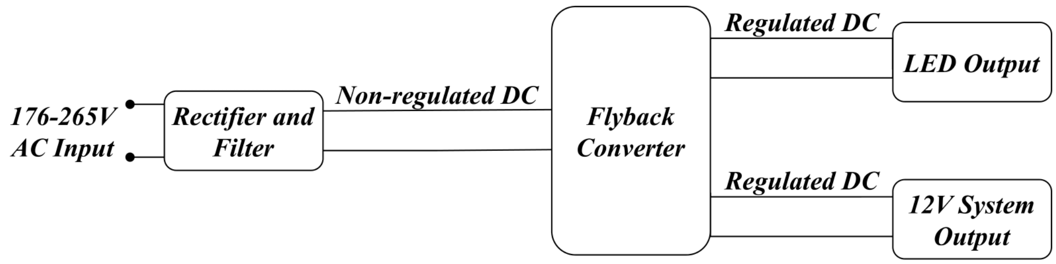

Figure 19 Proposed MOFC Block Diagram for TV Power Supply

As shown in Fig. 20, in the proposed model the boost bobbin, the boost MOSFET, and the diode are out of the circuit which are marked with the dashed red line. An extra N-MOS is added to the circuit to regulate the 12V system voltage which is marked with a solid green line. It is placed right after the diode of the 12V system winding output. The proposed model ensures that two outputs are regulated independently. Only one magnetic component is used and there is no need post regulator or an extra converter stage to supply a controlled current to the LEDs and 12V system voltage.

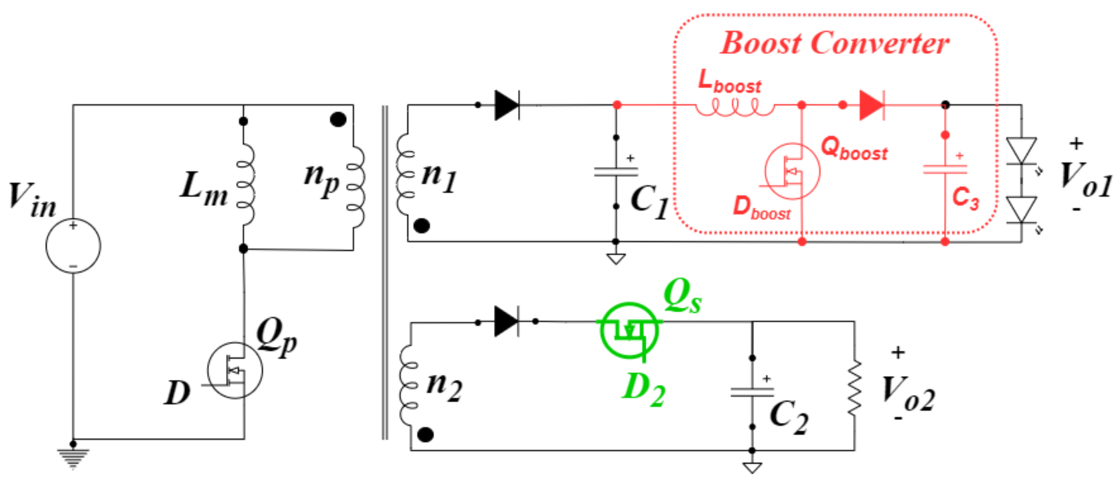

Figure 20 Proposed MOFC schematics for TV Power Supply

In the proposed model, FAN6300 PWM Controller is used on the primary side to control the primary MOSFET. On the secondary side, the MP4657A 4-String LED driver and system voltage controller [19] is used for individual control of both LED current and 12V system voltage. MP4657A outputs a gate signal to control the system MOSFET (Q_S) and regulates the 12V system voltage, and it also outputs a feedback signal to control the primary MOSFET (Q_P) through an opto-coupler.

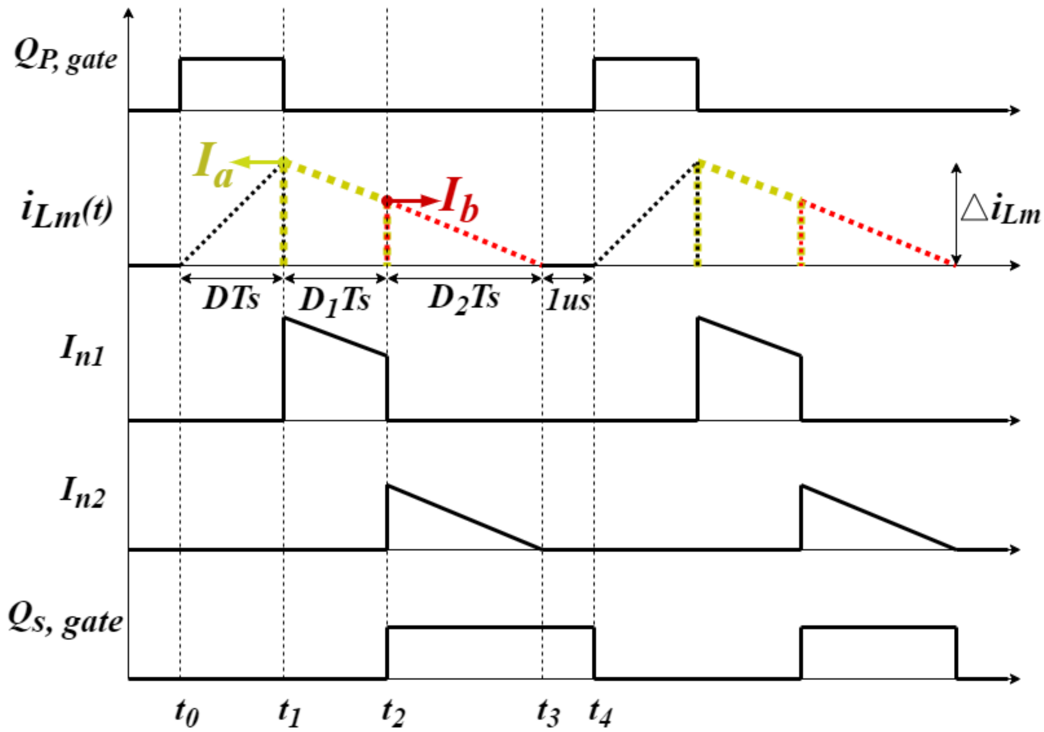

Figure 21 Switching Sequence of Proposed MOFC Model

The switching sequence is shown in Fig. 21. During $D{\times}Ts$, where D is the duty cycle of Q_P and where the switching period Ts is equal to $t_4 - t_0$, Q_P is ON, energy is stored in the magnetizing inductance of the transformer, and primary current ramps up. Since Q_S is OFF, energy is firstly transferred to the LED winding, and LED winding current linearly decreases. The controller monitors the minimum LED current and compares it with the set reference value, so it can control the flyback power and regulates the LED current. 12V system output is monitored by an external voltage divider and compared with a different reference value, and further regulates the system voltage through the duty cycle control of the Q_S. Since Q_S is ON, the rest of the energy is transferred to the 12V system winding. During $D_2 \times Ts$, the current linearly decreases. The gate signal of the Q_S is synchronized with Q_P. Therefore, Q_S turns off when the primary switch turns on. At this instantaneous, the secondary side current should be zero to achieve soft switching and avoid voltage spikes.

Working in DCM is the best option in order to ensure soft switching of system MOSFET. Because in DCM, the inductor current is discontinuous and it falls to zero. Switching a MOSFET when there is no current flow through on it, provides too low switching losses which increases the converter efficiency.

Chapter III

ANALYSIS AND DESIGN OF MODEL

3.1 Stages of Operation

The transformer of the proposed model contains 3 main power windings, the primary winding that stored the energy during Q_P is ON, secondary LED winding, and secondary system winding. Since the topology operates in DCM, there are three main intervals and one constant OFF time interval. The stages of the operation are shown in Fig. 22.

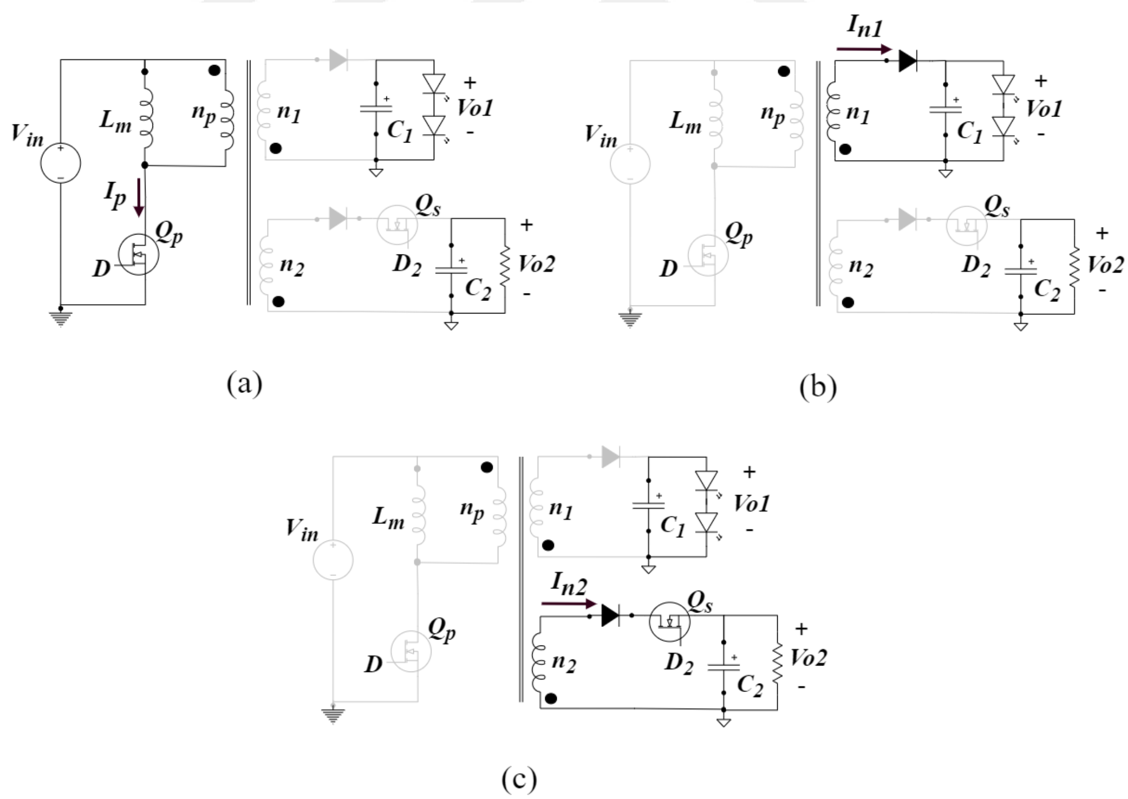

Figure 22 Operation stages of Proposed MOFC: (a) interval-1(t_0-t_1). (b) interval-2(t_1-t_2). (c) interval-3(t_2-t_3).

interval-1 [t_0<t<t_1] [see Figure 22(a)]: During $D{\times}Ts = t_1 - t_0$, Q_P is ON, and input current flows through the dotted terminal of the primary winding, so the polarity of the dot is positive. Since the dot is positive, there is no current flowing through the secondary windings because the rectifier diodes are reverse-biased. In this interval, energy is stored in magnetizing inductance, and the primary peak current is expressed as,

$$I_{p,peak} = I_a = \Delta i_{Lm} = \frac{V_{in} \times D \times T_s}{L_M} \tag{14}$$

Since the input voltage is constant, the primary current ramps up linearly. During Q_P conducts, the voltage across the magnetizing inductance is expressed as,

$$V_{LM}(t) = \frac{V_{in} \times L_M}{L_M + L_{leakage}} \tag{15}$$

Where $L_{leakage}$ is the leakage inductance of the primary winding, but it is negligible for this design since it is too small relative to magnetizing inductance. Therefore $V_{LM}(t)$ is equal to V_{in} during this interval.

Input power P_{in} is equal to the multiplication of the input voltage V_{in} and the average input current $I_{p,average}$. From the current waveform in Fig. 21, $I_{p,average}$ is calculated in eq. 16, and then P_{in} is expressed as follows,

$$I_{p,average} = \frac{V_{in} \times D \times T_s}{L_M} \times \frac{D \times Ts}{2} \times \frac{1}{Ts} = \frac{V_{in} \times D^2 \times T_s}{2 \times L_M} \tag{16}$$

$$P_{in} = V_{in} \times I_{p,average} = \frac{V_{in}^2 \times D^2 \times T_s}{2 \times L_M} \tag{17}$$

Derived from the eq. 17, the duty cycle D, can be expressed as,

$$D = \sqrt{\frac{P_{in} \times 2 \times L_M}{V_{in}^2 \times Ts}} \tag{18}$$

interval-2 [t_1<t<t_2] [see Figure 22(b)]: When Q_P is turned off at t_1, the stored energy is transferred to the secondary windings. Since Q_S is OFF, firstly LED winding is energized during $D_1 \times Ts = t_2 - t_1$, and current flows through the output capacitor C_1. In this interval LED current is controlled, therefore output is regulated successfully. Throughout this interval, no current flows through the system winding and the load of the system winding, which is the mainboard of the TV, is supplied by output capacitance C_2. During $D_1 \times Ts$, the voltage across magnetizing inductance L_M is expressed as,

$$V_{LM}(t) = -V_{o1} \times \frac{n_p}{n_1} \tag{19}$$

As can be seen from eq. 19, the output voltage is reflected to the primary side with respect to the turn ratio. And, the reflected voltage is negative because of the winding direction.

The average magnetizing inductance current I_{LM} during $D_1 \times Ts$ over a period is calculated from the area under $i_{Lm}(t)$ as shown in Fig. 21, and expressed as follows,

$$I_{LM,average} = \frac{I_a + I_b}{2} \times D_1 \times Ts \times \frac{1}{Ts} \tag{20}$$

The average LED winding current I_{o1}, and the output voltage V_{o1} during $D_1 \times Ts$ over a period can be written as follows,

$$I_{o1} = I_{LM,average} \times \frac{n_p}{n_1} = \frac{I_a + I_b}{2} \times D_1 \times \frac{n_p}{n_1} \tag{21}$$

$$V_{o1} = I_{o1} \times R_1 = \frac{I_a + I_b}{2} \times D_1 \times \frac{n_p}{n_1} \times R_1 \tag{22}$$

Derived from the eq. 21, the duty cycle of the LED winding D_1, can be expressed as,

$$D_1 = \frac{2 \times I_{o1}}{I_a + I_b} \times \frac{n_1}{n_p} \tag{23}$$

As can be seen from the formula, D_1 depends on the peak of the system winding current I_b. Calculation of the I_b will be given in the *interval-3*.

interval-3 [t_2<t<t_3] [see Figure 22(c)]: Q_S is turned on at time t_2, then the rest of the stored energy is transferred to the system winding. Once Q_S is turned on, it stays ON state until Q_P turns on. During $D_2{\times}Ts = t_3 - t_2$, the rectifier diode of LED winding is reverse-biased and there is no current flow through the LED winding. Only system winding is energized, and current flows through the system voltage output capacitor C_2. In this interval, the voltage across the magnetizing inductance is also reflected output voltage with respect to the turn ratio, and the sign is also negative because of the winding direction. $V_{LM}(t)$ can be written as,

$$V_{LM}(t) = -V_{o2} \times \frac{n_p}{n_2} \tag{24}$$

Since V_{o2} is constant during $D_2{\times}Ts$, magnetizing current decreases linearly as shown in Fig. 21, and the peak of the system winding current, I_b is expressed as,

$$I_b = \frac{V_{o2} \times D_2 \times T_s}{L_M} \times \frac{n_p}{n_2} \tag{25}$$

As can be seen from eq. 25, I_b depends on the duty cycle D_2. To get D_2, firstly we need to calculate the average system winding current I_{o2} which can be found from the average magnetizing current during $D_2{\times}Ts$ over a period,

$$I_{LM,average} = \frac{I_b}{2} \times D_2 \times Ts \times \frac{1}{Ts} \tag{26}$$

The average system winding current I_{o2}, and the output voltage V_{o2} during $D_2{\times}Ts$ over a period can be written as follows,

$$I_{o2} = I_{LM,average} \times \frac{n_p}{n_2} = \frac{I_b}{2} \times D_2 \times \frac{n_p}{n_2} \tag{27}$$

The output voltage V_{o2} can be expressed as follows,

$$V_{o2} = I_{o2} \times R_2 = \frac{I_b}{2} \times D_2 \times \frac{n_p}{n_2} \times R_2 \tag{28}$$

By substituting eq. 27 to eq. 28, V_{o2} is re-written as,

$$V_{o2} = \frac{V_{o2} \times D_2 \times T_s}{L_M} \times \frac{n_p}{n_2} \times D_2 \times \frac{n_p}{n_2} \times R_2 \tag{29}$$

Duty cycle D_2 is derived from the eq. 29 as follows,

$$D_2 = \sqrt{\frac{2}{R_2} \times \frac{L_M}{Ts} \times (\frac{n_2}{n_p})^2} \tag{30}$$

As can be seen from the formula, D_2 which is the duty cycle of the Q_S depends on the load, the magnetizing inductance, the period of the switching, and the turns ratio.

interval-4 [t_3<t<t_4]: Since the flyback works in DCM, the inductor current must fall to zero when the energy is transferred completely. As shown in Fig. 21, at t_3 instant, the energy transfer is done and therefore inductor current stays zero during $t_3<t<t_4$ interval. This interval is set by the controller for 1μs as a constant turn-off time to ensure the DCM mode of operation. However, the gate signal of Q_S is still high until Q_P turns on.

3.2 Design Consideration

Design specifications of the proposed Flyback converter are given in table 2. This proposed model is designed to operate in a wide voltage range of 176 - 264VAC. The line frequency range is 50 - 60Hz. Output power is defined according to the requirements of the TV structure. TV backlight unit requires 83V 500mA, and the mainboard of the TV requires 12.5V 2.5A for full load condition. The total output power P_{out} which is the sum of backlight unit output power $P_{out,1}$ and system output power $P_{out,2}$ is about 73W. Estimated efficiency, η is the ratio of total output power to input power as given in eq. 31.

$$\eta = \frac{P_{out}}{P_{in}} = \frac{P_{out,1} + P_{out,2}}{P_{in}} \tag{31}$$

In this design, η is taken 0.9. P_{in} is calculated 81W according to eq. 31.

Table 2 Design Specifications

Input Voltage Range, V_{in}	176 - 264 VAC
Line Frequency, f_{line}	50 - 60 Hz
Estimated Efficiency, η	0.9
Output Power, P_{out}	73W
Output 1, V_{o1}	0.5A 83V
Output 2, V_{o2}	2.5A 12.5V
Switching Frequency, f_{SW}	88kHz

In the very beginning of the design, DC input voltage range should be determined first. Minimum and maximum DC input voltage calculations are given in eq. 32 and eq. 33 respectively.

$$V_{DCmin} = \sqrt{2 \times V_{ACmin}^2 - \frac{P_{in} \times (1 - d_{charge})}{C_{in} \times f_{line}}} \tag{32}$$

Where V_{ACmin} is the minimum AC input voltage, f_{line} is the line frequency of AC input voltage, C_{in} is the input DC link capacitor, and d_{charge} is the DC link capacitor duty ratio, which is generally assumed as 0.2.

$$V_{DCmax} = \sqrt{2} \times V_{ACmax} \tag{33}$$

In this design, V_{DCmin} is calculated 195V, and V_{DCmax} is calculated 375V.

The voltage stress on the primary MOSFET depends on maximum input voltage, reflected voltage from secondary to primary, and voltage spikes due to parasitic effects. In flyback converter topology, the maximum drain-to-source voltage of the primary MOSFET V_{DSmax} is expressed in eq. 34.

$$V_{DSmax} = V_{DCmax} + V_R + V_{spike} \tag{34}$$

Where V_{DCmax} is the maximum DC input voltage, V_R is the output voltage reflected to the primary, and V_{spike} is the voltage spike that occurred when the MOSFET turned off instant due to parasitic effects of leakage inductance of the primary winding and parasitic capacitance that is the total capacitance on the primary MOSFET drain node.

Choosing V_R is a trade-off between voltage stresses of primary MOSFET and secondary diodes [20]. Too high V_R means higher turns ratio and V_{DSmax} but lower secondary diode stress. Too low V_R means lower turns ratio and V_{DSmax} but higher secondary diode stress [21]. V_R is defined as 105V at first.

V_{spike} is assumed 60V for this design. Note that V_{DSmax} is below %90 of the rated voltage of the primary MOSFET for safe operation. So that V_{DSmax} is 540V, the primary MOSFET should be chosen voltage rating 600V or higher.

3.2.1 Determination of D_{max} and L_M

In DCM operation, the maximum duty cycle must be determined at minimum DC input voltage at full loading condition.

$$D_{max} < \frac{V_R}{V_R + V_{DCmin}} \tag{35}$$

From eq. 35, D_{max} should be chosen lower than 0.35. Once the D_{max} is defined as 0.34, the minimum primary inductance of the transformer L_M is calculated as

$$L_M = \frac{(V_{DCmin} \times D_{max})^2}{2 \times P_{in} \times f_{SW}} \tag{36}$$

Switching frequency f_{SW} is 88kHz as given in table 3, P_{in} is specified in eq. 31, V_{DCmin} and D_{max} are specified in eq. 32 and eq. 35, respectively. The minimum L_M is calculated as 308uH.

The peak primary current $I_{p,peak}$ can be obtained in minimum DC input and full loading conditions. Since the inductor current falls to zero in DCM, $I_{p,peak}$ is equal to Δi_{LM} and it is expressed as

$$I_{p,peak} = \Delta i_{LM} = \frac{V_{DCmin} \times D_{max}}{L_M \times f_{SW}} \tag{37}$$

From the eq. 37, estimated maximum primary peak current, $I_{p,peak}$ is calculated 2.44A.

3.2.2 Transformer Parameters

In order to choose the proper core type and size, manufacturers' core catalogs are helping a lot. The proper core should be selected according to the input voltage range, output power, number of converter outputs, and switching frequency. In this project, EQ3014 core is chosen.

Applying the transformer core parameters B_{sat} is the saturation flux density in $tesla$, and A_e is the cross-sectional area of the core in mm^2 which are given in Table 3, the minimum number of turns for the primary winding to avoid the core saturation is expressed as

$$n_{p,min} = \frac{L_M \times I_{p,peak}}{B_{sat} \times A_e} \times 10^6 \quad (turns) \tag{38}$$

Here $n_{p,min}$ is calculated 29 turns. After some iterations, the number of turns for the primary winding is chosen 32 turns. With the chosen n_p and chosen core, the magnetizing inductance L_M is obtained 325uH. The chosen core structure and the complete flyback transformer are depicted in Fig. 23 below.

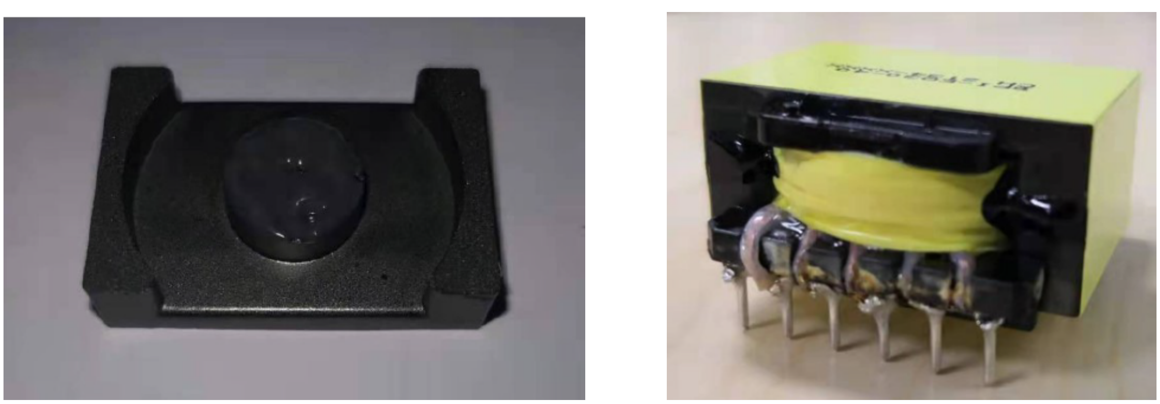

(a) (b)

Figure 23 Flyback transformer: (a) EQ30 core structure; (b) the complete flyback transformer

Once the number of the primary winding turns is defined, the number of secondary winding turns can be calculated as

$$\frac{n_p}{n_1} = \frac{V_R}{V_{o1} + V_{diode}} \tag{39}$$

Where V_{diode} is the forward voltage of the rectifier diode and V_R is the LED output voltage reflected to the primary. The number of LED winding turns n_1 is determined as 22 turns, and the turn ratio between the LED winding and the system winding is expressed as

$$\frac{n_1}{n_2} = \frac{0.85 \times (V_{o1} + V_{diode})}{V_{o2} + V_{diode}} \tag{40}$$

Here %15 margin is advised to ensure DCM operation and for better compensation and reliable system operation [19]. From the eq. 40, number of system winding turns n_2 is obtained as 5 turns.

3.2.3 System MOSFET Ratings

After turn ratios are defined, the voltage stress on the Q_S must be considered to select the proper MOSFET. The maximum voltage stress on the Q_S occurs at the maximum input AC voltage. Considering the parasitic effects and derating of the MOSFET, %20 margin is advised for more safe operation. The maximum voltage rating of Q_S is expressed in eq. 41.

$$V_{max,Q_S} = \frac{V_{ACmax} \times n_2}{0.8 \times n_p} \tag{41}$$

$V_{max,Qs}$ is calculated as 52V. The average current flow through Q_S is equal to the output current which is the system current of 2.5A. But this current is a pulse waveform, its RMS value is 1.5-2 times of the average current. For choosing the proper MOSFET, the current rating must be 2-3 times the RMS current. To calculate $I_{RMS,Qs}$, firstly we need to get D_2 and $I_{n2,peak}$. D_2 is calculated from eq. 30, as 0.528. To calculate $I_{n2,peak}$, I_b must be known. I_b is calculated from eq. 25, as 1.477A.

Table 3 Design Parameters

Primary Inductance, L_M	325uH
Transformer Core	EQ30
Saturation Flux Density, B_{sat}	0.25T
Cross-sectional Area of the Core, A_e	108 mm^2
Number of Primary Turns, n_p	32
Number of LED winding Turns, n_1	22
Number of System Winding Turns, n_2	5
Primary MOSFET, Q_P	600V 20A N-Channel
System MOSFET, Q_S	100V 50A N-Channel

The peak of the system winding current $I_{n2,peak}$ can be expressed and calculated as

$$I_{n2,peak} = I_b \times \frac{n_p}{n_2} = 1.477 \times \frac{32}{5} = 9.45A \tag{42}$$

$I_{RMS,Qs}$ can be calculated from the triangular shape shown in Fig. 21, as expressed in eq. 43.

$$I_{RMS,Q_S} = I_{n1,peak} \times \sqrt{\frac{D_2}{3}} = 9.45 \times \sqrt{\frac{0.528}{3}} = 3.96A \tag{43}$$

The switching loss of this MOSFET is too low because of the soft switching. However, conduction loss should be taken into account due to $R_{DS,ON}$. In this design, 100V 50A N-Channel D-PAK MOSFET is used with $R_{DS,ON}$ is 10.2mOhm. The conduction power loss of system MOSFET is calculated as,

$$P_{loss,Q_S} = I^2_{RMS,Q_S} \times R_{\mathrm{DS,ON}} = 3.96^2 \times 0.0102 = 160mW \tag{44}$$

In order to validate the design calculations, calculated duty cycles, peak currents, and output powers are compared to the measured and simulated values in table 4. All calculations are done at the 320VDC input voltage and full loading condition.

3.2.4 Circuit Schematic of Proposed TV Power Supply

The proposed power supply circuit is drawn in the Xpedition Designer package program of Mentor Graphics. The circuit schematic of the proposed model is given in

Fig. 24. AC-DC rectifier block, flyback transformer and MOSFET, controller ICs, outputs, and feedback structure is shown separately.

EMI filter is used at the AC input to avoid electromagnetic radiation. The AC input voltage 176-264VAC is rectified by the bridge rectifier and the DC voltage is charged to the bulk capacitors.

The primary side of the transformer has two windings; one is the main primary winding which transfers the energy, second winding is the auxiliary winding which supplies 12-18V to the flyback controller IC. Thus the auxiliary winding has a low number of turns. The secondary side of the transformer has two windings; one is the 12V system winding and the other one is the LED winding.

Flyback MOSFET is driven by the flyback controller IC. Following the source of the MOSFET there are current sense resistors that are 1206 size SMD and parallel to each other. The primary current is monitored by the controller CS pin from the voltage that occurred on the current sense resistors during the primary switch ON time. CS pin data contributes to the generation of the PWM signal with the feedback data and also over current protection (OCP).

On the secondary side, the 12V system output is rectified by three parallel ultra-fast diodes and has a system MOSFET for regulation. The LED output is rectified by two ultra-fast diodes. The LED driver and system voltage controller IC is supplied by the 12V system output. It monitors the out voltages of two winding and returning currents of the LEDs. According to monitored current and voltage levels, IC outputs a gate signal to control the system MOSFET which regulates the 12V system voltage, and feedback signal OPT which is sent to the primary flyback controller IC by an optocoupler. This IC can control the LED's current by using digital PWM dimming. According to the applied duty ratio of the PWM signal, it adjusts the amount of current that flows into LED pins.

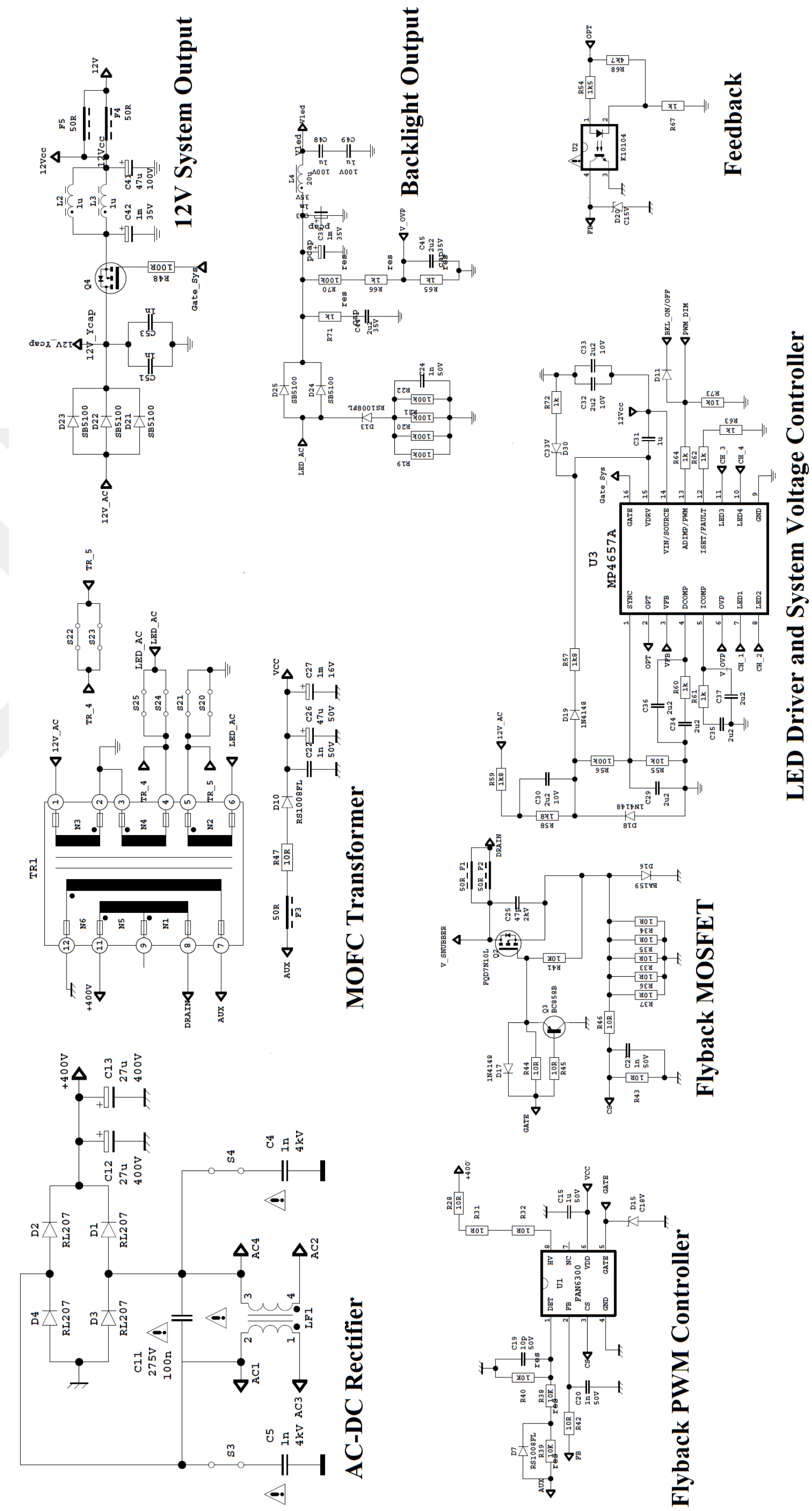

Figure 24 Schematic of Proposed MOFC

Chapter IV

RESULTS

4.1 Simulation Results

The proposed model is simulated in the Simulink package program of Matlab. The proposed model circuit is constructed as given in Fig. 25 according to design specifications and design parameters which are given in table 2 and table 3 respectively.

The input voltage is set to 320VDC. The system winding output supplies 12.13V @2.502A to the mainboard of the TV which is modeled by a resistor. 1000uF electrolytic capacitor is preferred to reduce output voltage ripple. The LED winding output supplies 83.17V @0.501A to the backlight of the TV which is modeled by a resistor. 560uF electrolytic capacitor is preferred here because the current drawn by the LEDs is not quite large. The rectifier diodes and MOSFETs are modeled ideally.

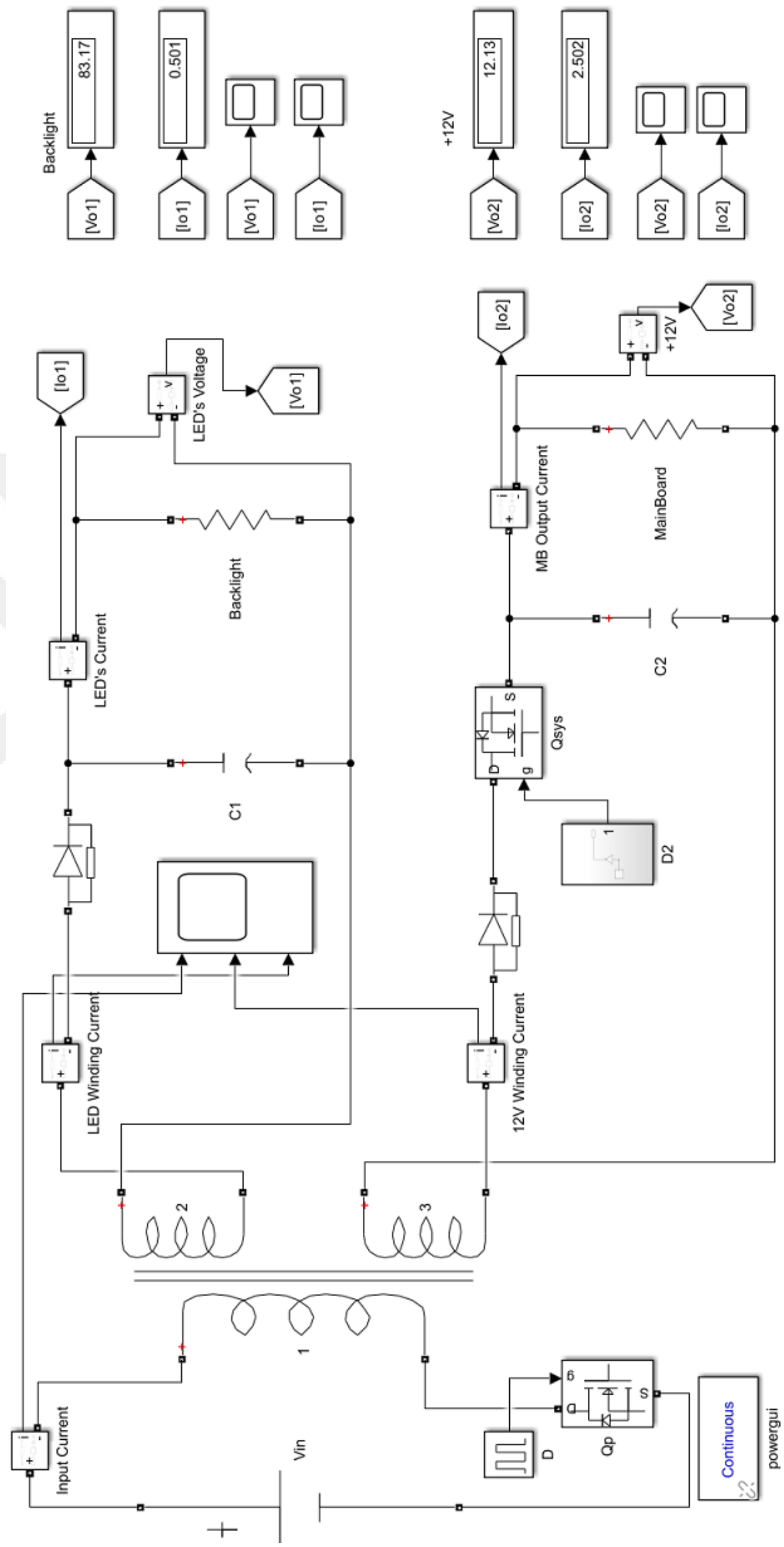

Figure 25 Simulation Model of the Proposed MOFC

Transformer winding currents are given in Fig. 26. When the primary switch is turned on, the primary current ramps up as marked with the black line. After the primary switch is turned off, the stored energy is transferred to the LED winding since the system MOSFET which is modeled as Qsys in the simulation model is off. The orange line represents the LED winding current. This current is rectified by the diodes and the output capacitor is being charged. When the Qsys is turned on, the rest of the stored energy is transferred to the 12V system winding. The 12V system winding current is represented by the red line. The peak values of the winding currents and the duty ratios are given in table 5.

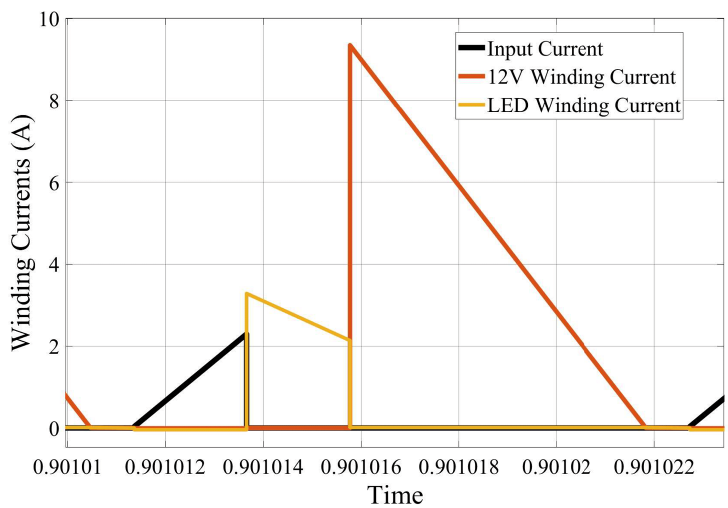

Figure 26 Simulation of transformer winding currents

12V system output voltage and its ripple are given in Fig. 27. In the simulation the system output supplies 12.13V @2.5A. There is a small overshoot and then the voltage reaches its steady-state level in 200ms. The output voltage ripple is around 15mV. Output ripple may be affected by the output capacitor and its inner resistance and inductance values which are known as equivalent series resistance (ESR) and equivalent series inductance (ESL) respectively. Here in the simulation capacitors are ideal. Fig. 28 shows the system output current and its ripple. The current ripple behavior is the same as the voltage ripple since the load is resistive.

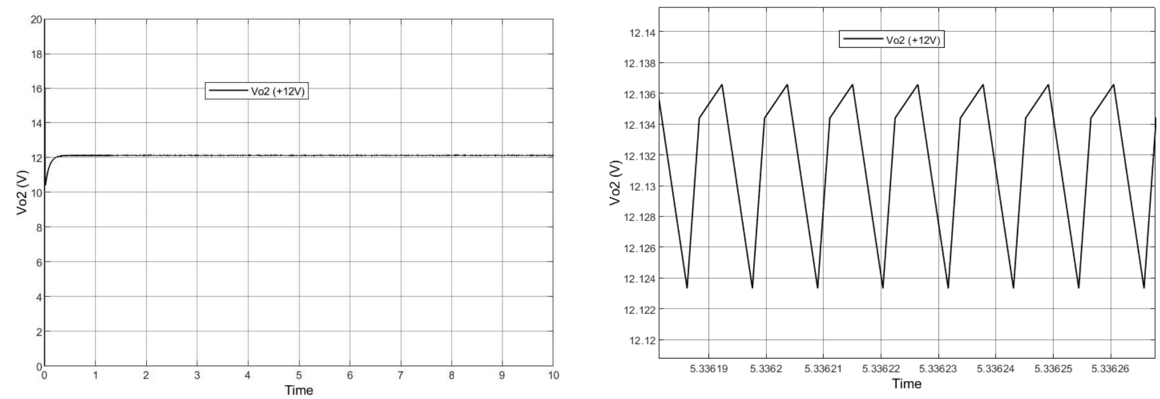

(a) (b)

Figure 27 Simulation of 12V system output: (a) 12V system output voltage; (b) system output voltage ripple

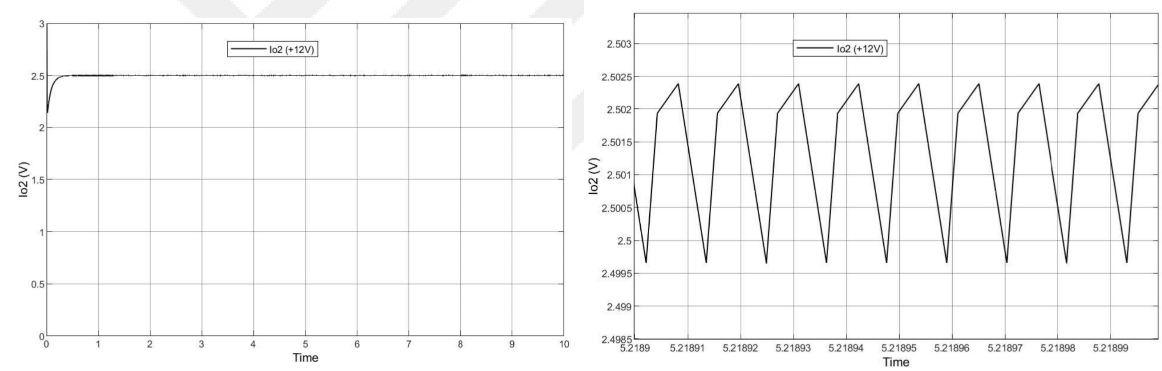

(a) (b)

Figure 28 Simulation of 12V system output: (a) 2.5A system output current; (b) system output current ripple

LED winding output voltage and its ripple are given in Fig. 29. In the simulation the LED output supplies 83.17V @0.5A. The overshoot at the start-up is acceptable and it reaches the steady-state level in 300ms. The output voltage ripple level is around 10mV. Fig. 30 shows the 500mA LED output current and its ripple.

Both the 12V system output voltage and the LEDs current are regulated well as seen in the simulation results. Fig. 26 shows that the 12V system winding current peak value is way higher than the others. This means thermal problems may occur

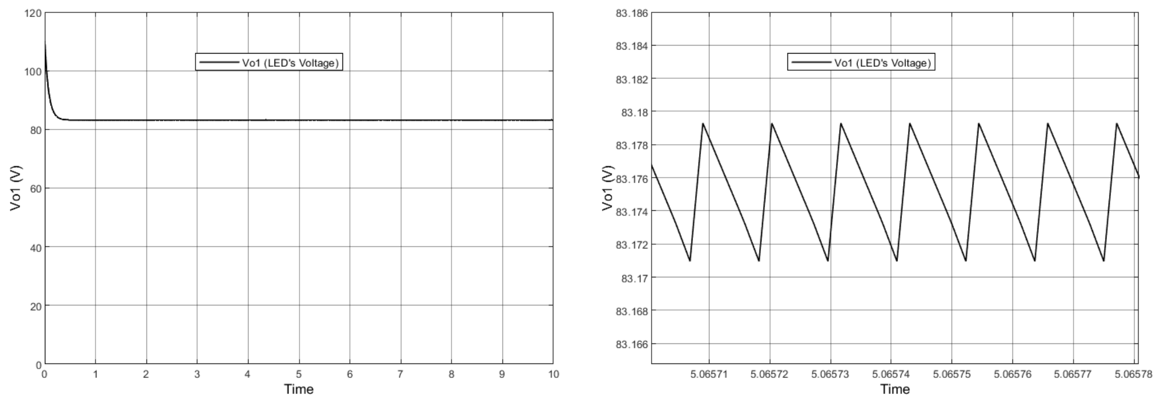

(a) (b)

Figure 29 Simulation of LED output: (a) LED output voltage; (b) LED output voltage ripple

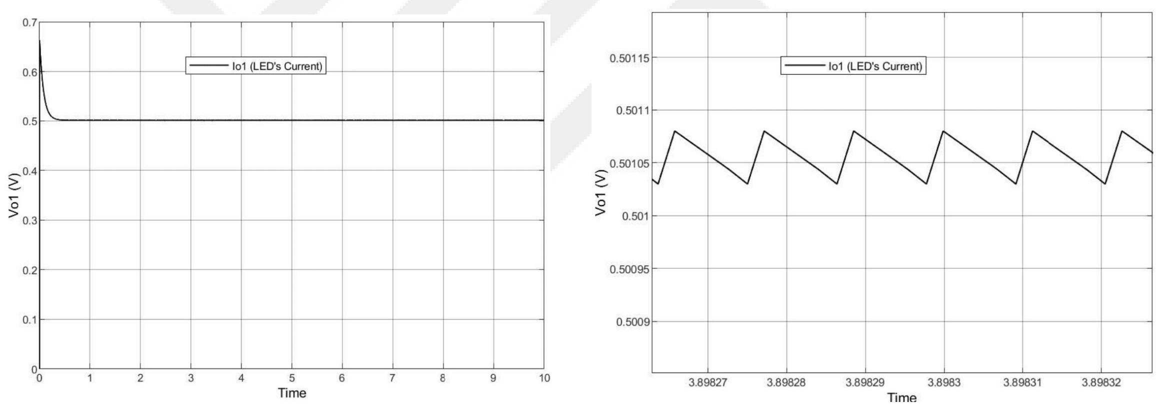

(a) (b)

Figure 30 Simulation of LED output: (a) LED output current; (b) LED output current ripple

since the load needs 2.5A continuously. That's why the rectifier diodes of the 12V output must have a low forward voltage drop and the system MOSFET must have a low drain-source on resistance. To avoid thermal problems three pieces of ultra-fast diodes are used in parallel in the hardware implementation. And MOSFET is chosen with the on-resistance of 10mOhm.

4.2 Experimental Results

The experimental setup is set in the VESTEL laboratory. The drawn schematic circuit of the proposed model in Fig. 24 is printed on PCB. Hardware implementation of the proposed model is constructed according to design specifications and design parameters which are given in table 2 and table 3 respectively. The complete design of the proposed power supply card and the measurement setup is shown in Fig. 31.

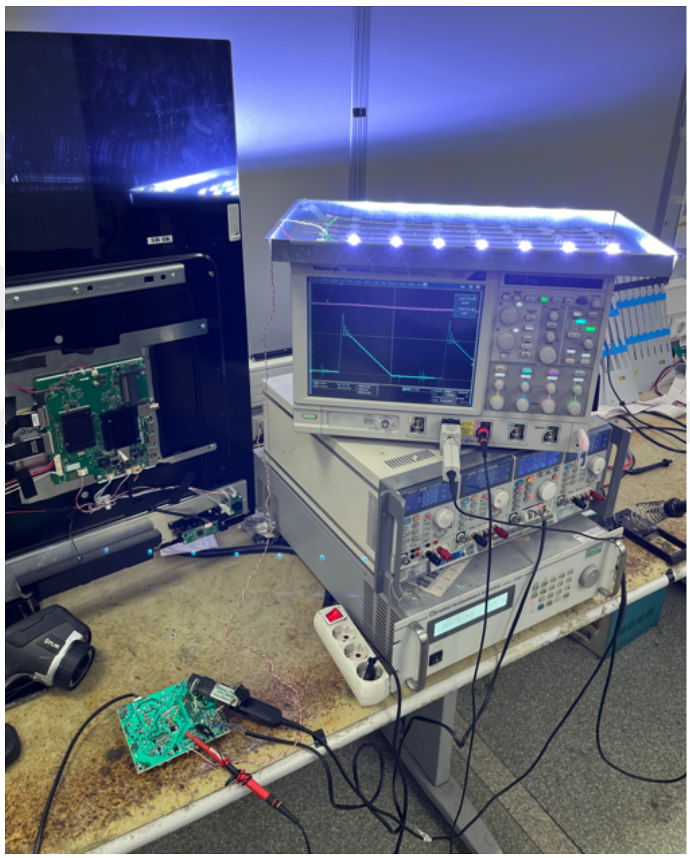

Figure 31 Proposed power supply and the measurement setup

The power supply card is supplied from an AC Variac. At the outputs, Prodigit electronic load is used for loading 2.5A from the 12V system output, and LED strings of a 43" TV panel are used for loading 83V 0.5A from the LED output of the power supply card.

In order to make sensitive measurements Tektronix DPO 7104C oscilloscope whose sample rate is up to 20GS/s is used. All measurements are done at room temperature.

The transformer winding currents are measured as given in Fig. 32.

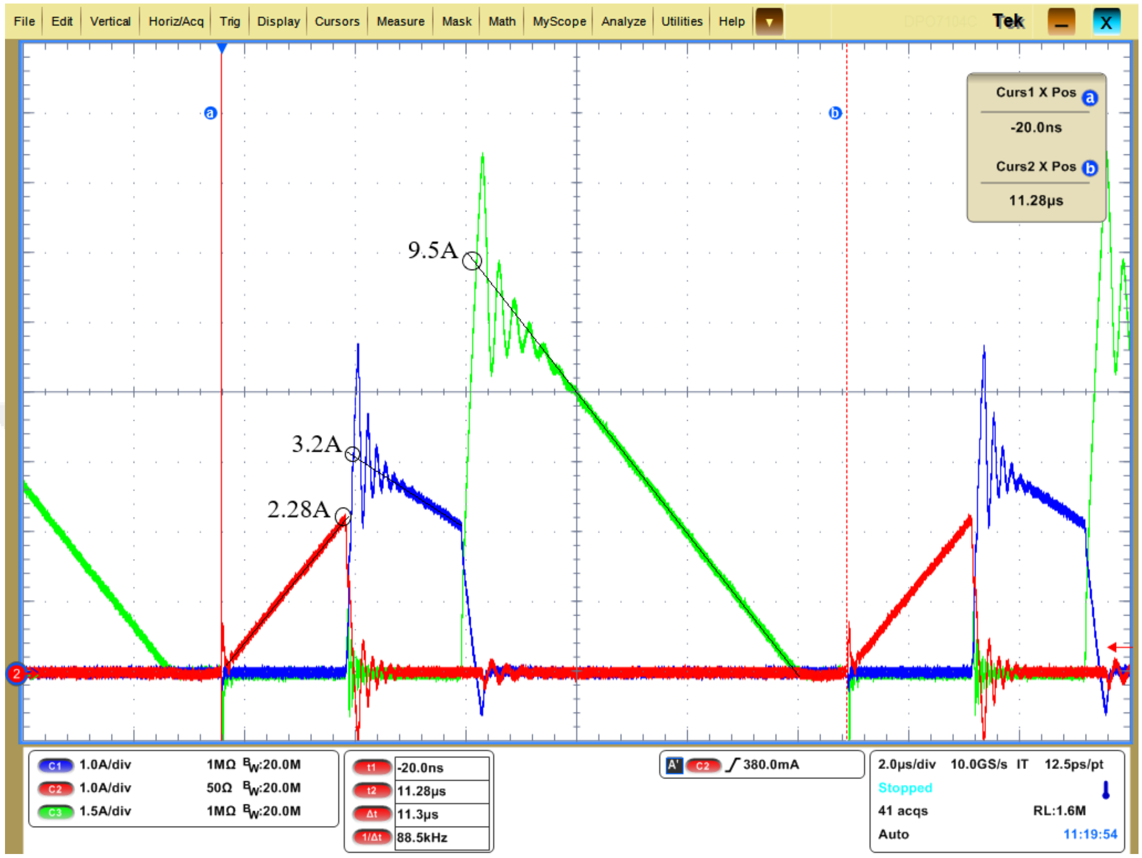

Figure 32 Measured transformer winding currents

Channel1 (C1, Blue): The LED winding current

Channel2 (C2, Red): The primary winding current

Channel3 (C3, Green): The 12V system winding current

As calculated and simulated previously, the primary current rams up during on-time, and the LED winding current is created when the primary switch is turned off, there is no energy transfer to the 12V system winding since the system MOSFET is off. The 12V system winding current starts conduction when the system MOSFET is turned on. There is a constant 1 micro-second off-time for the primary switch before the start of each switching cycle to ensure DCM mode of operation.

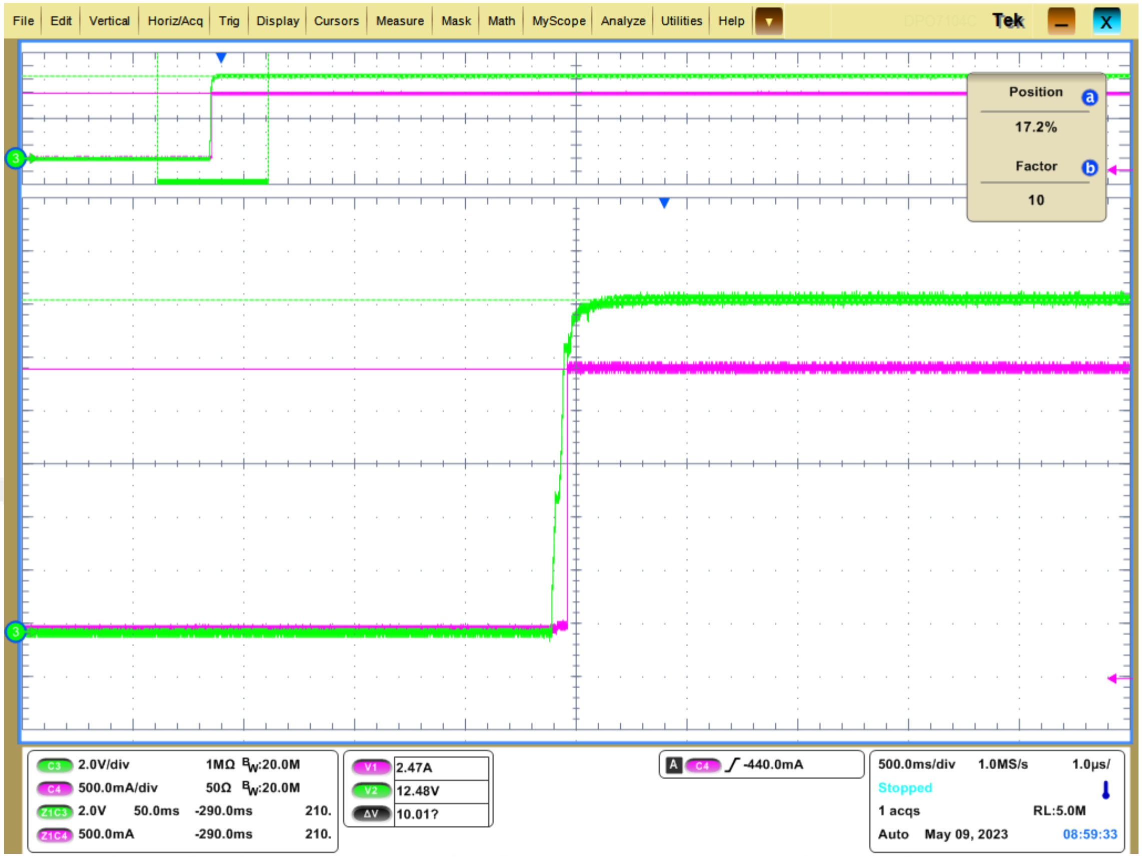

Figure 33 Measured 12V system output voltage and current at start-up

Channel3 (C3, Green): 12V system output voltage

Channel4 (C4, Pink): 12V system output current

12V system output voltage is measured as 12.48V at full loading condition as given in Fig. 33. In the hardware, a 1000uF electrolytic capacitor with a low ESR value is used to get a low ripple at the output. No over-shoot occurred at the start-up instant of 12V in laboratory measurement.

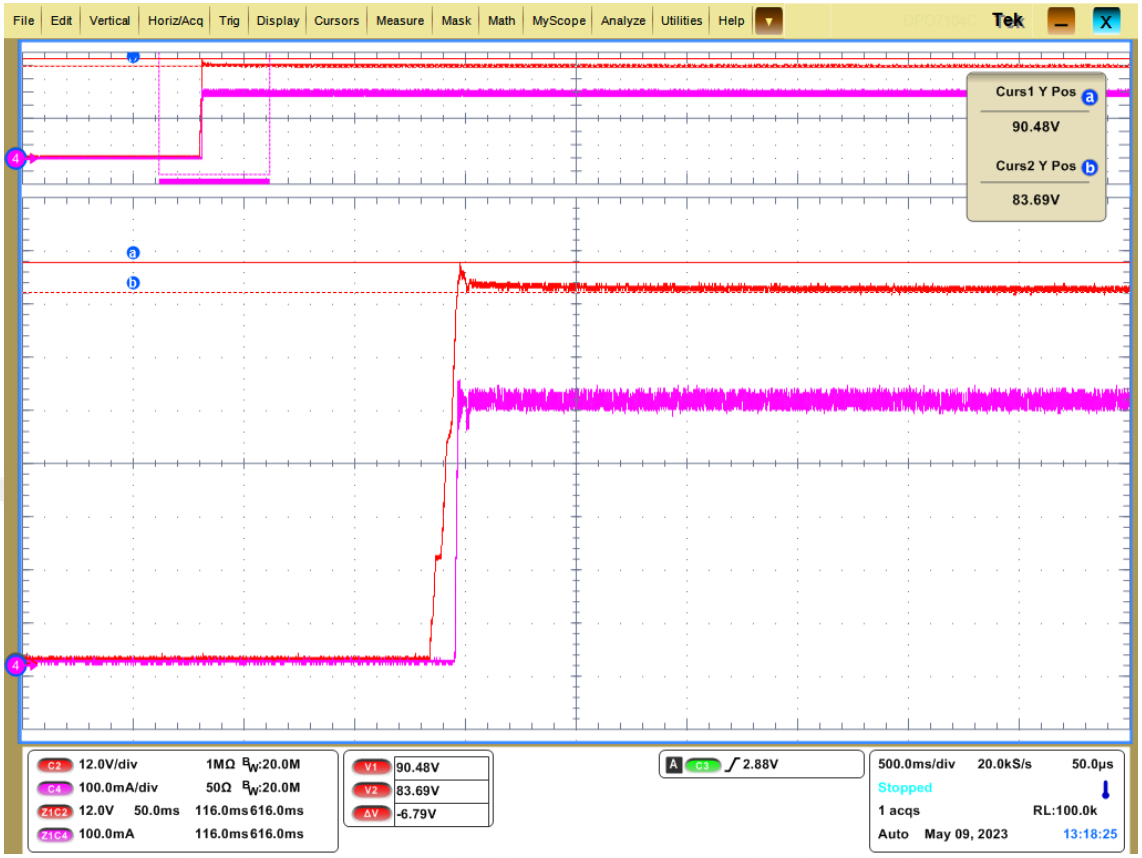

Figure 34 Measured LED output voltage and current at start-up

Channel2 (C2, Red): LED output voltage

Channel4 (C4, Pink): LED output current

The LED output voltage and current are measured at the start-up instant at full loading condition as given in Fig. 34. This voltage level may vary a few volts because the LED's forward voltage is affected by the temperature. Due to the nature of the LEDs, there appears a small overshoot at start-up. In the hardware, 1 micro-Henry bobbin is used to avoid electromagnetic radiation. And, a 560uF electrolytic capacitor with a low ESR value is used to get a low ripple at the output.

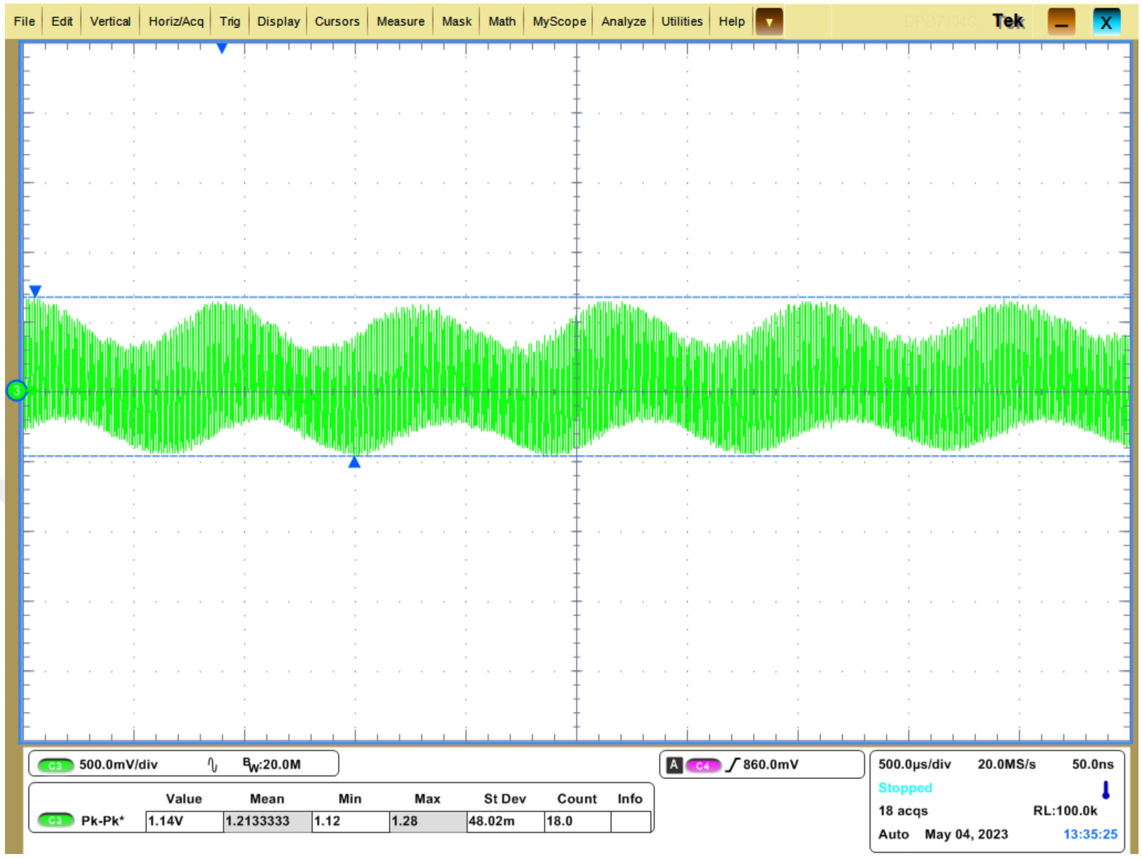

Figure 35 Measured LED output voltage ripple

Channel3 (C3, Green): LED output voltage ripple

The ripple measurement of LED output voltage is given in Fig. 35. Peak-to-peak 1.14V ripple is measured at the LED output voltage. This level corresponds to %1.36 ripple level.

The drain-source voltage of the primary switch and primary current waveforms are given in Fig. 36. The voltage appears on the switch when the switch is off. There are two clamp levels; one is around 440V which is the sum of the input voltage and reflected voltage of LED winding during system MOSFET is off, and the other one is 400V which is the sum of the input voltage and reflected voltage of 12V system winding during system MOSFET is on.

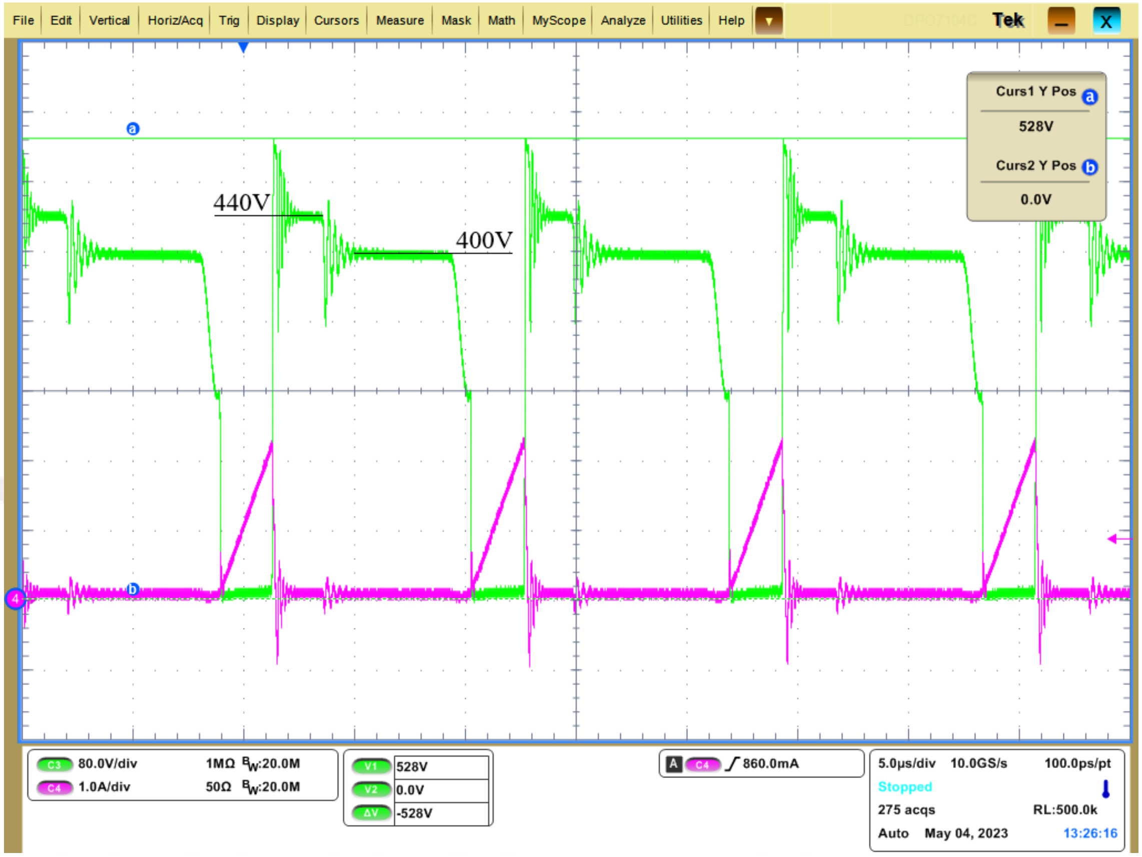

Figure 36 Drain-source voltage of primary switch and primary winding current

Channel3 (C3, Green): Drain-source voltage of primary switch

Channel4 (C4, Pink): Primary winding current

The voltage stress on the primary switch is measured from the drain to the source of the MOSFET. The maximum voltage is measured as 528V when the switch is turned off. As given eq. 34 in section 3, voltage spikes and oscillations occur because of leakage inductance and parasitic capacitances. To decrease this stress, the leakage inductance is decreased by rearranging the transformer windings each other. The distances were taken into account to decrease parasitic effects during designing the layout of the PCB.

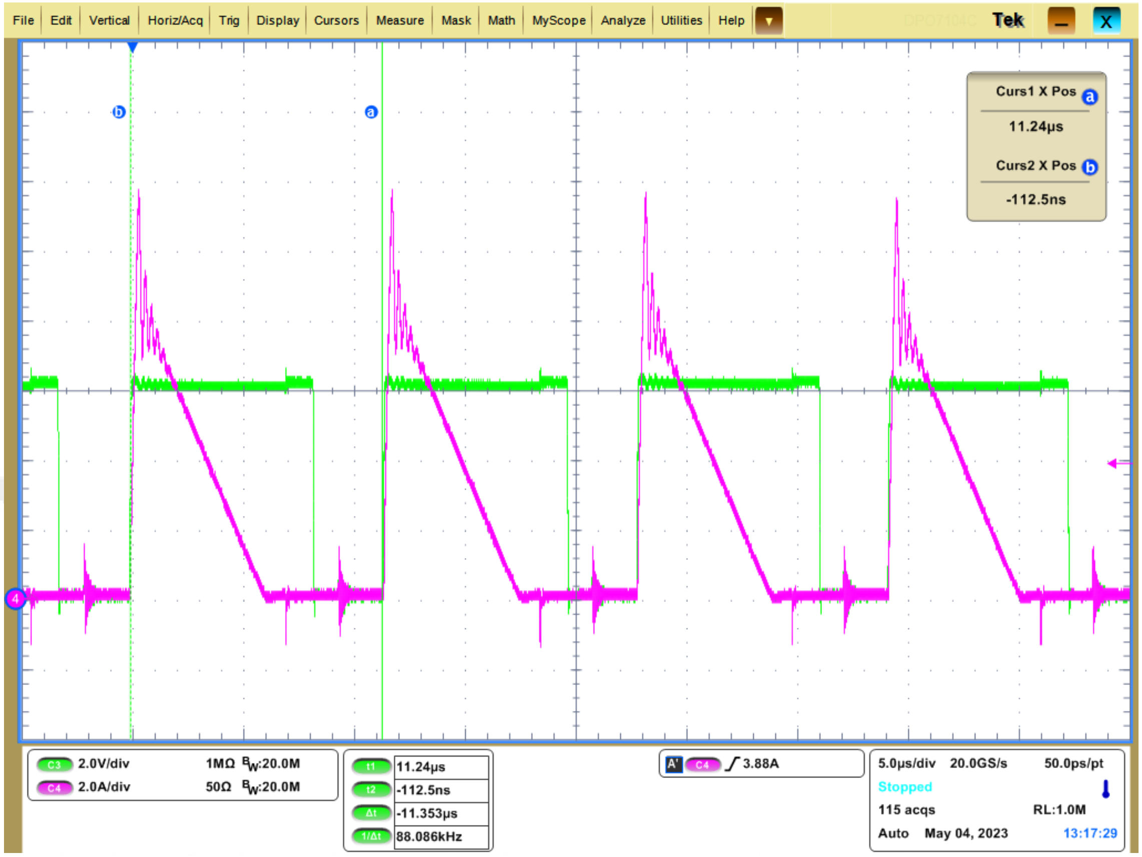

Figure 37 Gate-source voltage of system MOSFET and 12V system winding current

Channel3 (C3, Green): Gate-source voltage of system MOSFET

Channel4 (C4, Pink): 12V system winding current

The gate-source voltage and 12V system winding current waveforms are given in Fig. 37. The rest of the stored energy transfer starts when the system MOSFET is turned on. However, the switch is still on even if the energy transfer is done when the current decreases to zero. Because the turn-off time of this switch is synchronized with the turn-on time of the primary switch. So the system MOSFET is turned off when the primary switch is turned on.

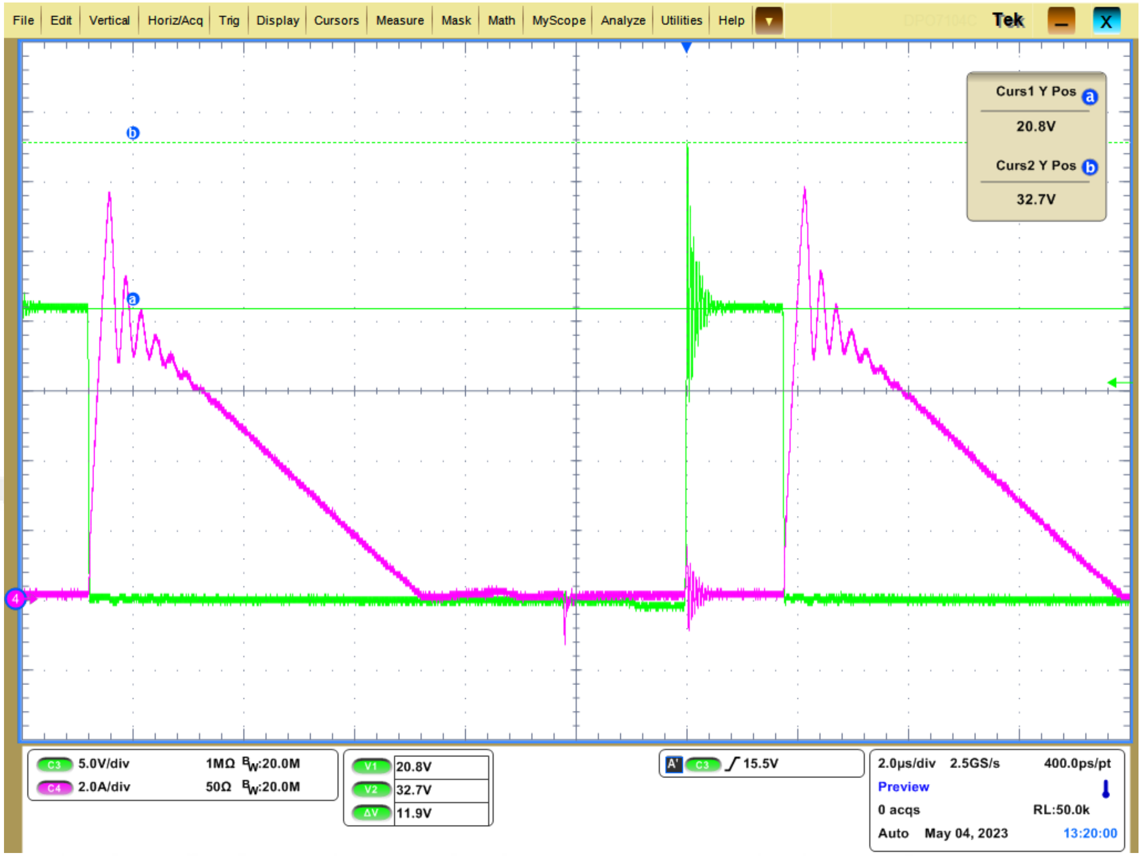

Figure 38 Drain-source voltage of system MOSFET and 12V system winding current

Channel3 (C3, Green): Drain-source voltage of system MOSFET

Channel4 (C4, Pink): 12V system winding current

The drain-source voltage and 12V system winding current waveforms are given in Fig. 38. The maximum voltage stress of the system MOSFET is calculated in eq. 41 in section 3. In the laboratory, the maximum level is measured as 32.7V. The clamp voltage level of 20.8V appears during the switch is off. This voltage is the reflected voltage from the LED winding.

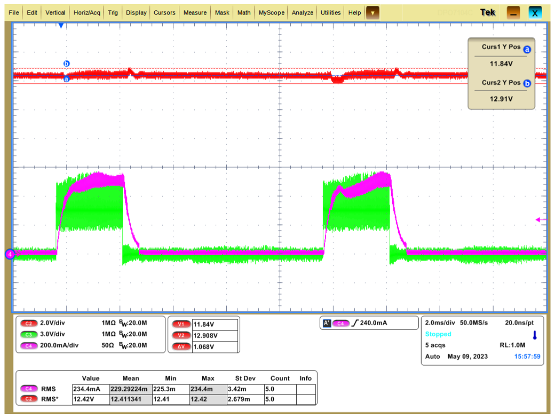

(a)

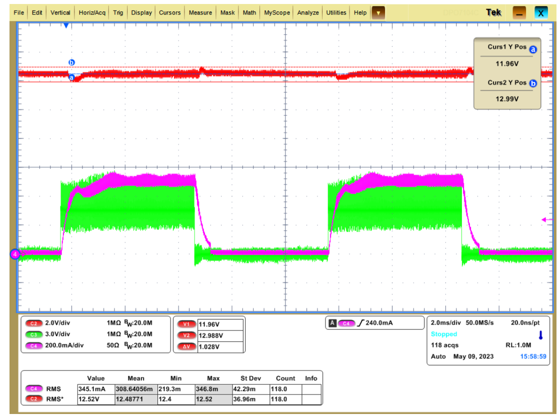

(b)

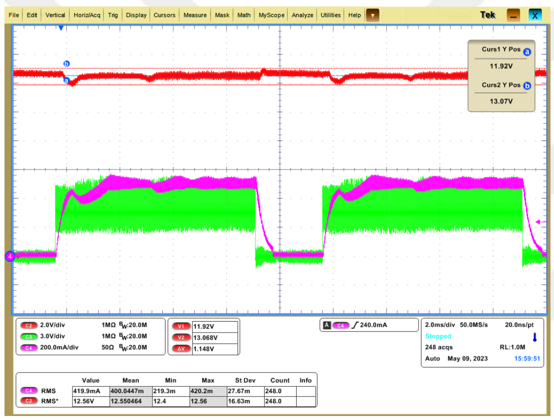

(c)

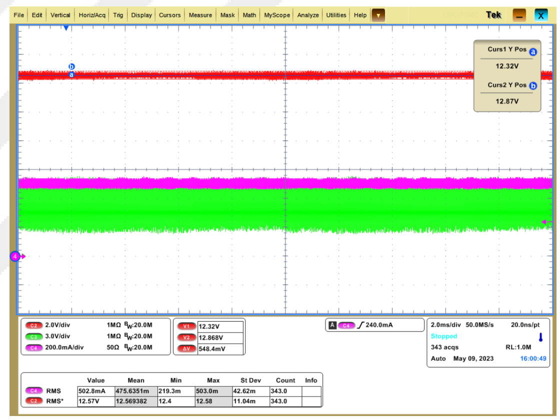

(d)

Figure 39 12V system output voltage response to the change in LED current when 12V is loaded 2500mA (a) Duty of PWM dimming is %25; (b) Duty of PWM dimming is %50; (c) Duty of PWM dimming is %75; (d) Duty of PWM dimming is %100

Channel2 (C2, Red): 12V system output voltage

Channel3 (C3, Green): PWM signal

Channel4 (C4, Pink): LED output current

The response of 12V output voltage, when 12V is loaded 2500mA, is given in Fig. 39 according to the different duty ratios of PWM dimming signals applied to the PWM input of the LED driver and system controller IC.

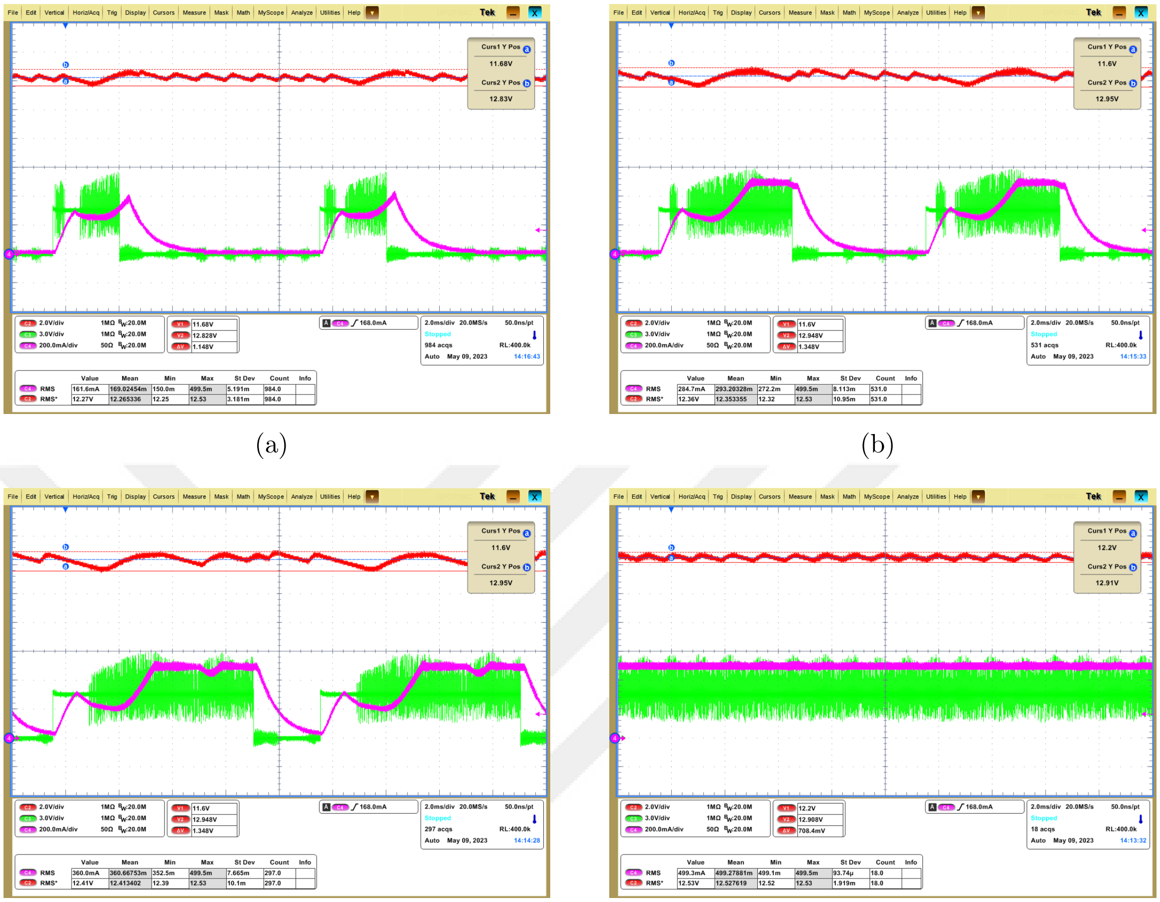

(a) (b) (c) (d)

Figure 40 12V system output voltage response to the change in LED current when 12V is loaded 500mA (a) Duty of PWM dimming is %25; (b) Duty of PWM dimming is %50; (c) Duty of PWM dimming is %75; (d) Duty of PWM dimming is %100

Channel2 (C2, Red): 12V system output voltage

Channel3 (C3, Green): PWM signal

Channel4 (C4, Pink): LED output current

The response of 12V output voltage, when 12V is loaded 500mA, is given in Fig. 40 according to the different duty ratios of the PWM dimming signal. In this test, we can see that the converter can regulate both 12V output voltage and LEDs current. The ripple calculation of each loading is given in table 4. 12V regulation in light loads is not as tight as the full load. When the 12V output is loaded 500mA and the LED current is dimmed by %50, the ripple level of 12V is ±%5.61 which is the worst case. The best regulation is provided as ±%2.28 when 12V output is fully loaded and the LED current is driven with the %100 duty of the PWM signal.

Table 4 Percentage of 12V ripple for different loading conditions

Load of 12V output / Duty of PWM (%)	500mA	2500mA
25	±%4.78	±%4.45
50	±%5.61	±%4.28
75	±%5.61	±%4.78
100	±%2.95	±%2.28

4.2.1 Thermal Measurements

Thermal measurement of the proposed power supply card is done in room conditions as an open frame as shown in Fig. 41. The power supply card output is fully loaded 73W with an input voltage of 230VAC, and the measurements are done after one hour because the temperatures can reach a steady point around one hour generally since there is no airflow in the ambient. The temperature of the flyback transformer and the flyback mosfet is measured at 69.4 and 74 in Celsius respectively.

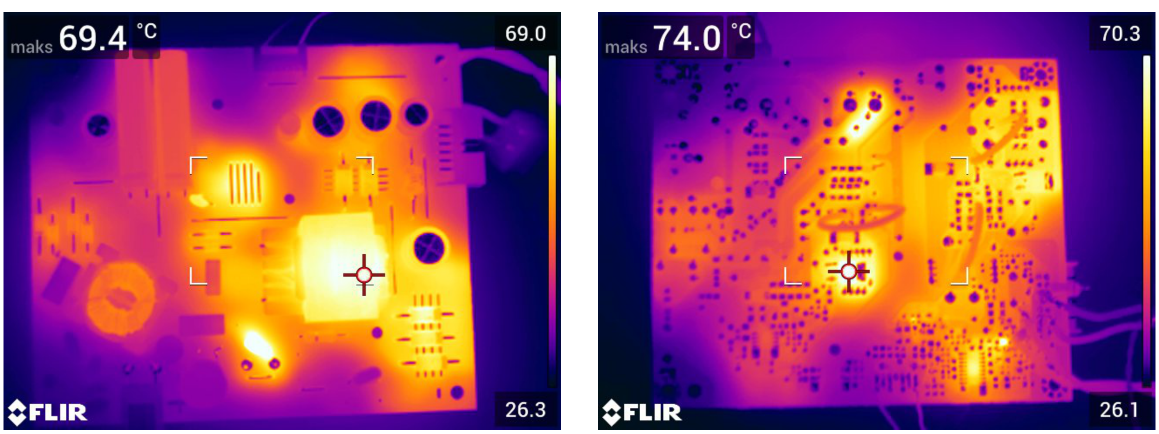

(a) (b)

Figure 41 Thermal measurement of proposed power supply card: (a) top side; (b) bottom side

4.2.2 Validation and Comparisons

In order to validate the proposed model, calculated duty cycles and peak of the transformer winding currents are compared to simulated and measured values in table 5.

Table 5 Calculated, Simulated, and Measured Values

	D	D_1	D_2	$I_{p,peak}$ (A)	$I_{n2,peak}$ (A)	$P_{out,1}$ (W)	$P_{out,2}$ (W)
Calculated	0.21	0.18	0.52	2.34	9.45	41.4	31.43
Simulated	0.20	0.18	0.52	2.31	9.51	41.67	31.35
Measured	0.20	0.18	0.52	2.28	9.50	41.9	31.3

The design parameters of the proposed model are first calculated, then it is simulated in Matlab Simulink, and finally implemented in hardware. The results in Table 5 are quite similar. This validation is supported by simulating and measuring the transformer winding currents waveforms. Apart from the oscillations observed in the measured waveforms compared to the simulation waveforms, the model is verified and validated.

Thanks to the lack of a boost converter stage on the secondary side, the peak efficiency increases while card sizes significantly decrease. Conventional model card sizes are $170mm \times 118mm \times 15mm$ which are length, width, and height, respectively. This card is designed to supply about 73W output which corresponds to the power density of 0.242 W/cm^3. The peak efficiency of the conventional model is measured %89.5. The proposed model is also designed to supply about 73W output power by the decreased sizes to $130mm \times 110mm \times 15mm$. As a result, the proposed model is %28.8 smaller than the conventional model which is capable of giving the same output power. And, power density is increased to 0.340 W/cm^3 while the peak efficiency is increased to %90.85.

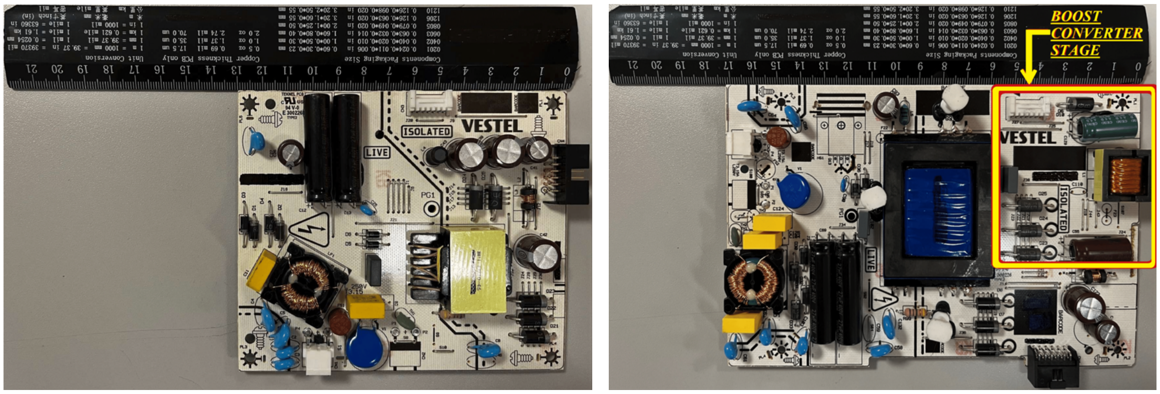

(a) (b)

Figure 42 TV power supply cards: (a) Proposed power supply card; (b) Conventional power supply card

4.2.3 Cost Comparison

The cost comparison between the conventional and proposed models is given in table 6. The table includes only the components that make a price difference. Due to the boost converter stage being out of the circuit, the prices of the boost bobbin, boost diode, and boost MOSFET are out of the BOM list. Thanks to the lack of the boost converter, PCB size decreased by %23, so the price of it decreased as well. The main transformer core is smaller which helps decrease the costs. LED driver ICs have the same number of pins, but MP4657A is a bit cheaper. In the proposed model side, only the system MOSFET is extra. As a result, the proposed model is 0.46$ cheaper than the conventional existing model.

Table 6 Cost comparison between the conventional and proposed models

Models / Components	Conventional Model	Proposed Model
PCB	0.38\$ (FR1, 200.6cm^2)	0.27\$ (FR1, 143cm^2)
Transformer	0.76\$ (EFD43 Core)	0.60\$ (EQ30 Core)
LED Driver IC	0.30\$ (AL3066)	0.20\$ (MP4657A)
Boost bobbin	0.17\$ (25uH 20x20x10mm^3)	-
Boost diode	0.02\$ (DO201 3A/200V)	-
Boost MOSFET	0.20\$ (FDD390N15 21A/150V)	-
Sytem MOSFET	-	0.30\$ (FDD86110 50A/100V)
Total	1.83\$	1.37\$

Chapter V

CONCLUSION

In this project, the design of a multiple-output flyback converter with independently controlled outputs for a TV power supply is presented. A 43” LED TV needs a power supply card that can supply the mainboard system and LED backlight of the TV. Generally, the mainboard system of TVs requires 12V, while the LED backlight requires a controlled current supplied within the range of 40V-100V, which can vary based on the LED structure and TV size. Conventional power supply cards are capable of providing 12V from the flyback transformer. However, they achieve voltages of 24V or 36V by doubling or tripling the main winding and then boosting it to the LED voltage level using an additional converter stage cascaded after the flyback stage. This extra converter stage increases the card sizes and costs while decreasing the overall efficiency. In the proposed model, the mainboard system and the LED backlight are supplied from the flyback transformer directly.

The proposed model is analyzed, simulated, implemented in hardware, and tested. In Section 2 and Section 3, operation stages and design considerations are explained in detail. According to calculated values, the simulation setup is prepared in Matlab Simulink. The proposed model is simulated according to design specifications and design parameters which are given in table 2 and table 3, respectively. The simulation results are reported and current and voltage waveforms are given. Simulation results verify the working principle of the proposed model.

After the model is verified with the simulation, the schematic of the model and layout is drawn in the Xpedition Designer program. The circuit is printed to PCB, and the components that are used in hardware implementation are chosen according to calculated limitations. The experimental setup is set in the VESTEL laboratory. The proposed power supply card is energized and tested in different loading conditions. Measurements are reported in detail in Section 4. Measurement of transformer winding currents verifies the working principle of the proposed model. The peak currents, duty cycles, and output powers are compared in table 5. Measurements are quite similar to the calculated and simulated values.

The independent control of the outputs is achieved for a TV power supply. To measure the regulation, 12V output voltage is observed in detail with different loading situations. At first, 12V output is loaded 500mA for light loading conditions. Then the ripple level of 12V is measured for four different duty ratios of the PWM signal that is applied to the LED driver IC PWM pin to determine the LED's output current level. The worst regulation is obtained as ±%5.61 for PWM duty ratios of %50 and %75. Then 12V output is loaded 2500mA for full loading conditions. The best regulation is obtained as ±%2.28 for PWM duty ratio of %100 which drives the LED's current fully.

The thermal performance of the proposed power supply is obtained in room conditions. The power supply is fully loaded at the input voltage of 230VAC. The flyback transformer is measured 69.4 Celcius. The flyback MOSFET is measured 74.0 Celcius. These measurements are quite acceptable for a TV power supply card. There is no abnormal temperature has occurred.

The peak efficiency of the proposed card is measured %90.85. The power density of the proposed card is 0.340 W/cm^3. By comparing to the existing conventional model, efficiency is increased by %1.35, and power density is increased by %28.8. The costs of the boost converter are out of the BOM list, and also smaller PCB and transformer reduced the BOM costs. As given in table 6, the overall power card cost is reduced 0.46$ which corresponds to %11.8 cost reduction. A more compact power supply card design for a TV with higher efficiency and lower cost is achieved.

Appendix A

APPENDIX

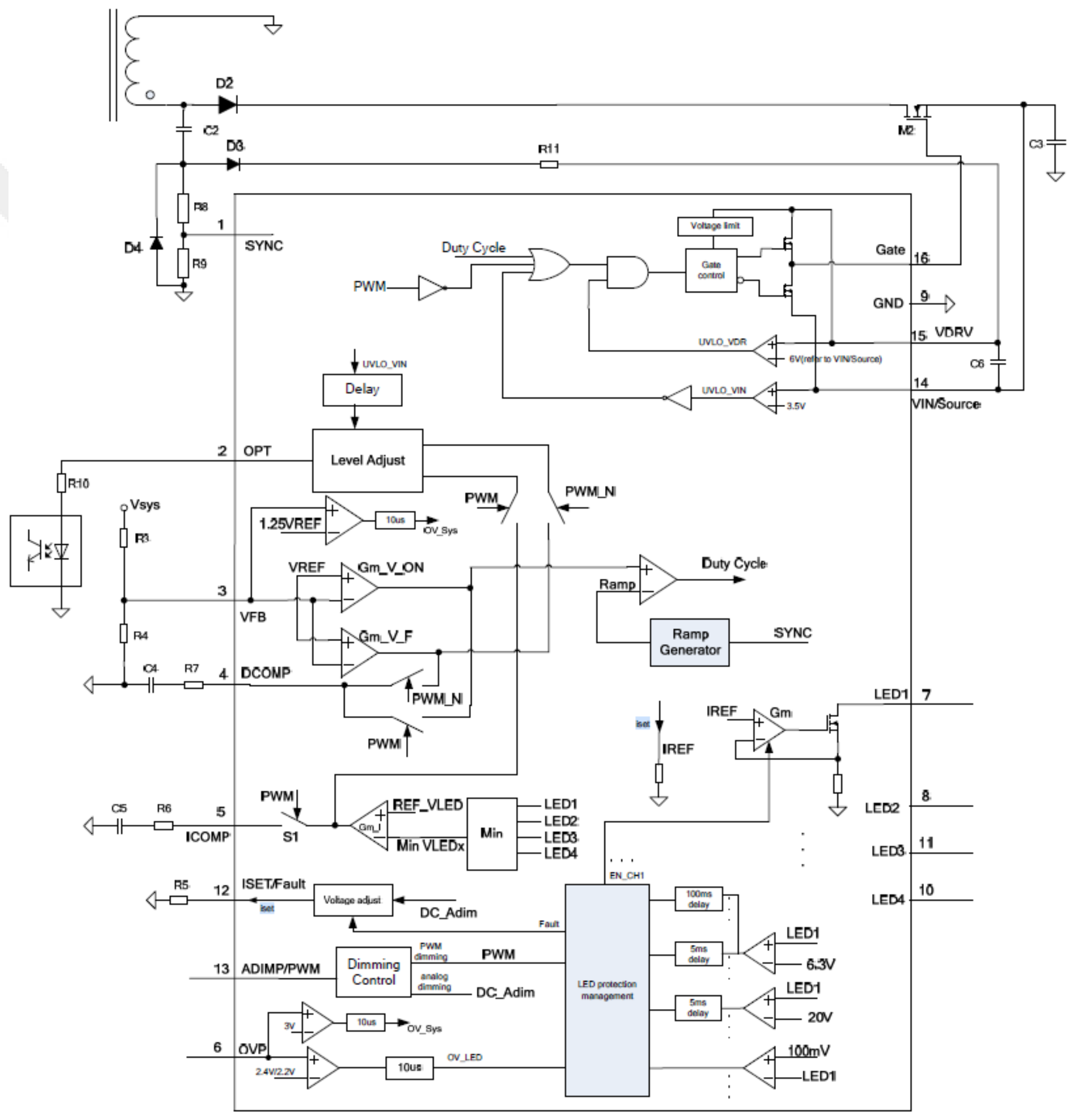

Figure 43 Functional block diagram of LED driver and system MOSFET controller IC MP4657A

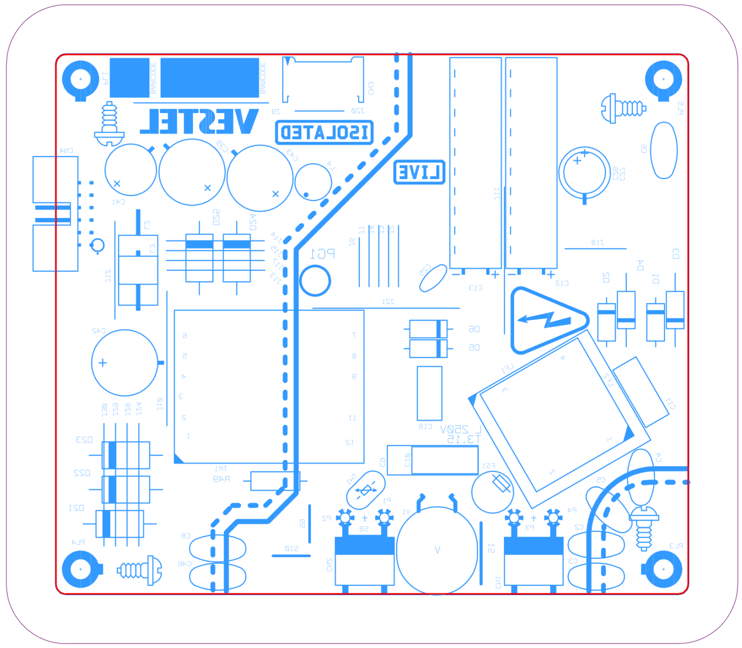

Figure 44 Top side placement of layout of proposed power supply card

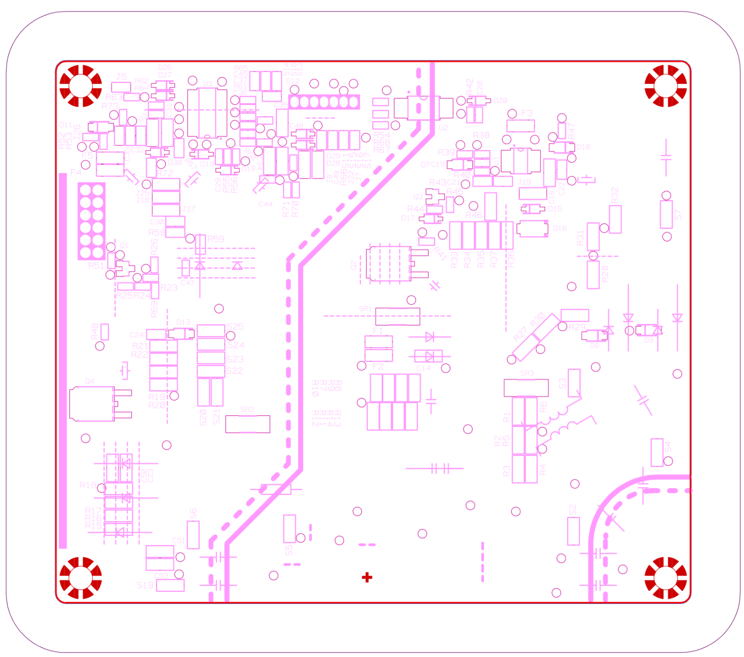

Figure 45 Bottom side placement of layout of proposed power supply card

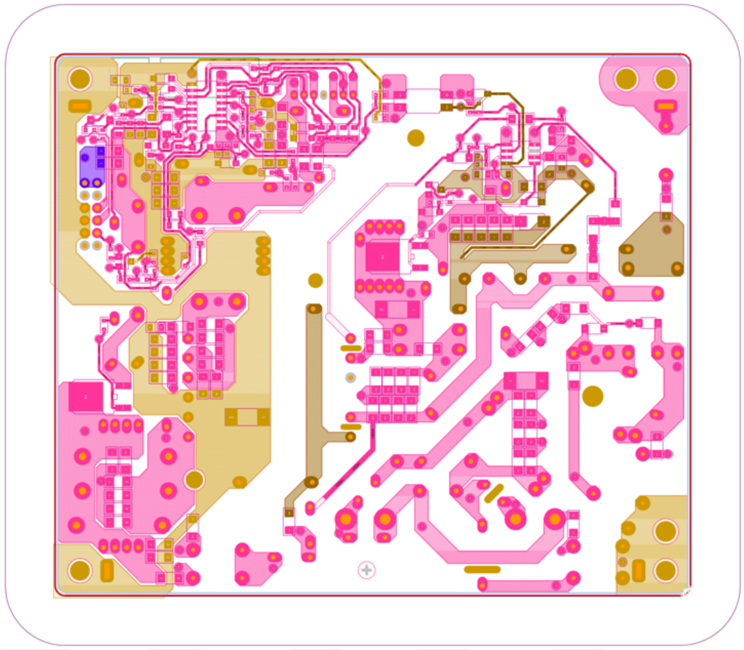

Figure 46 PCB layout paths

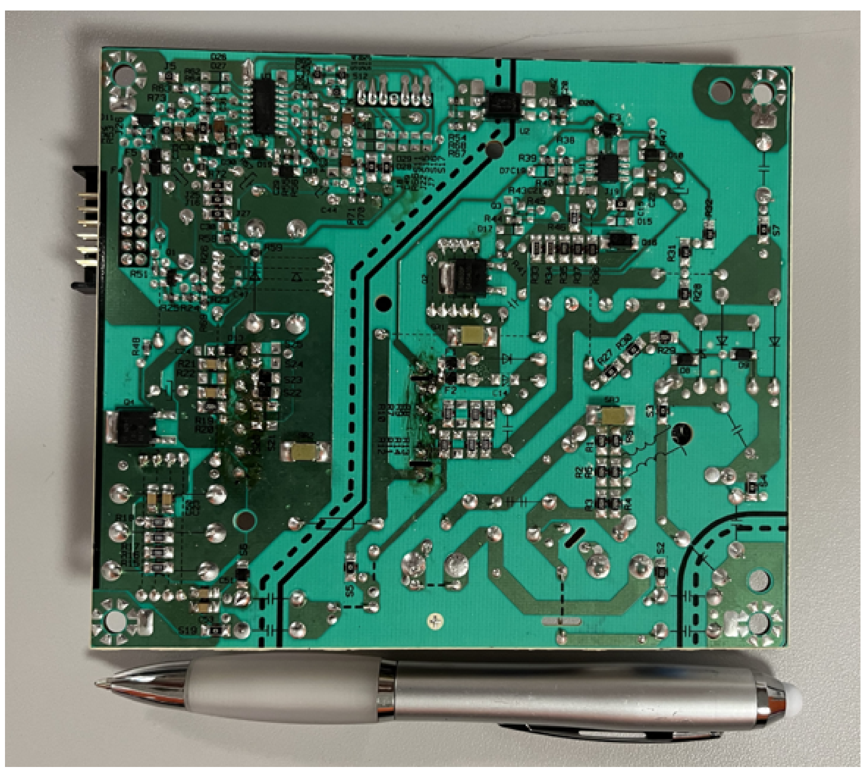

Figure 47 Bottom side of proposed power supply card

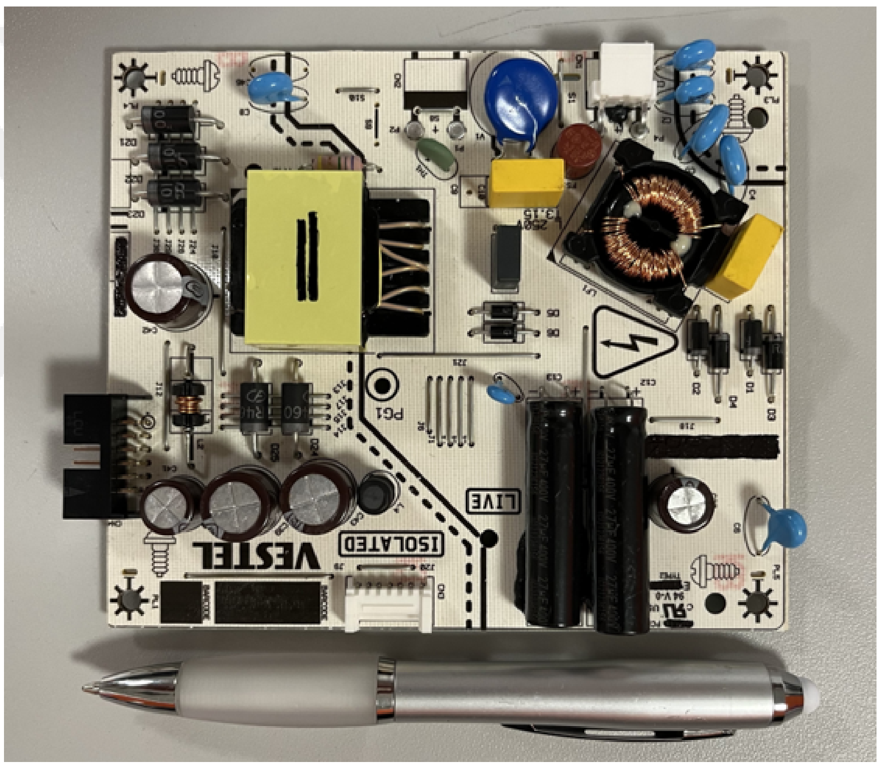

Figure 48 Top side of proposed power supply card

REFERENCES

[1] P.R.W. Burns, "The first demonstration of television," IET, vol.21, pp.953-956, October 1975.

[2] R.C. Webb, "Tele-Visionaries: The People Behind the Invention of Television," 2005.

[3] R. P. H. Adji and S. Ismail, "Design of cathode ray tube analyzer and rejuvenator for CRT and CRO," TENCON IEEE Region 10 Conference, Macao, China, 2015, pp. 1-5, doi: 10.1109/TENCON.2015.7373135.

[4] M. Shiomi et al., "A fully digital convergence system for projection TV," in IEEE Transactions on Consumer Electronics, vol. 36, no. 3, pp. 445-453, Aug. 1990, doi: 10.1109/30.103158.

[5] J. K. Lim et al., "New cost-effective driving circuit for plasma-TV," Digest of Technical Papers International Conference on Consumer Electronics, Las Vegas, NV, USA, 2009, pp. 1-2, doi: 10.1109/ICCE.2009.5012182.

[6] J. -W. Jung, "A novel cost-effective driving scheme with fewer power devices for plasma TVs," in IEEE Transactions on Consumer Electronics, vol. 55, no. 2, pp. 583-590, May 2009, doi: 10.1109/TCE.2009.5174426.

[7] LG e-book "LCD Direct View LED and OLED Explained," 2016.

[8] Y. Ishii, "The World of Liquid-Crystal Display TVs—Past, Present, and Future," in Journal of Display Technology, vol. 3, no. 4, pp. 351-360, Dec. 2007, doi: 10.1109/JDT.2007.909381.

[9] James Singh, K.; Huang, Y.M.; Ahmed, T.; Liu, A.C.; Huang Chen, S.W.; Liou, F.J.; Wu, T.; Lin, C.C.; Chow, C.W.; Lin, G.R.; et al. "Micro-LED as

a promising candidate for high-speed visible light communication," Appl. Sci. 2020, 10, 7384. https://doi.org/10.3390/app10207384.

[10] Ned Mohan, T. M. Undeland, W.P. Robbins "Power Electronics; Converters, Applications, and Design" third edition, John Wiley and Sons, USA, 2003.

[11] Ibrahim Kaya "A Switch Mode Power Supply for Producing Half Wave Sine Output", Middle East Technical University, June 2008.

[12] Daniel W. Hart "Power Electronics," McGraw-Hill, 2011.

[13] Abdi Ahmed, A. Kosar "Analysis and Design of Multioutput Flyback Converter," Chalmers University of Technology, Gothenburg, Sweden 2016.

[14] Marian K. Kazimierczuk "Pulse-width Modulated DC-DC Power Converters," John Wiley and Sons, USA, 2008.

[15] Muhammad H. Rashid "Power Electronics; Devices, Circuits, and Applications" fourth edition, Pearson Education, 2014.

[16] Jean Picard,"Under the Hood of Flyback SMPS Designs," . Texas Instruments, Power Supply Design Seminar, USA: Wiley, 2011.

[17] A. Sarkar, B. T. Vankayalapati and S. Anand, "GaN-Based Multiple Output Flyback Converter With Independently Controlled Outputs," in IEEE Transactions on Industrial Electronics, vol. 69, no. 3, pp. 2565-2576, March 2022, doi: 10.1109/TIE.2021.3066928.

[18] N. Vazquez, H. Lopez, C. Hernandez and H. Calleja, "Multiple-output DC-to-DC based on the flyback converter," 2008 11th IEEE International Power Electronics Congress, 2008, pp. 105-108, doi: 10.1109/CIEP.2008.4653820.

[19] MP4657A Pure Single Stage Flyback 4-String LED Driver and System Voltage Controller, pp.19-20, available at www.monolithicpower.com, April 2020 (accessed October 21, 2020).

[20] Application Note AN-4150, pp5-6, available at www.fairychildsemi.com, 2006 (accessed March 14, 2022).

[21] Allan A. Saliva, "Design Guide for Off-line Fixed Frequency DCM Flyback Converter." Infineon Technologies North America (IFNA) Corp., pp6-7, V1.0, available at www.infineon.com, 2013 (accessed March 15, 2022).

[22] A. A. Mohammed and S. M. Nafie, "Flyback converter design for low power application," 2015 International Conference on Computing, Control, Networking, Electronics and Embedded Systems Engineering (ICCNEEE), 2015, pp. 447-450, doi: 10.1109/ICCNEEE.2015.7381410.

[23] "The History of How We Play - Pixel Pushing" available at www.thehistoryofhowweplay.wordpress.com, May 2018 (accessed April 16, 2023).

[24] "EPSON 3LCD Projector Technology", available at www.epson.com.au, 2011 (accessed April 16, 2023).

VITA

Mr. Ramazan Düzgün graduated from Isparta Yalvac Atatürk Anatolian High School in 2014. Then, he obtained his bachelor's degree in Electrical and Electronics Engineering from Dokuz Eylül University Faculty of Engineering in 2019. After graduating, he began working as a power electronics designer in the TV Power R&D team at VESTEL Electronics. He commenced his M.Sc. degree at Ozyegin University in 2020. His research interests lie in power electronics and electric vehicles. Currently, he is involved in designing Mobile TV adapters, E-bike battery chargers, OLED and MiniLED TV power supplies, and LED driver cards.